Study of an upwelling event in the Portuguese coast

Upwelling Filaments in Aveiro region

Paulo Filipe Alexandre Correia

Thesis to obtain the Master of Science Degree in

Engenharia do Ambiente

Supervisors: Prof. Dr. Aires José Pinto dos Santos and Profª. Drª.Lígia Laximi Machado de Amorim Pinto

Examination Committee

Chairperson: Professor Doutor Ramiro Joaquim de Jesus Neves

Supervisor: Professor Doutor Aires José Pinto dos Santos

Member of committee: Doutor Paulo Nogueira Brás de Oliveira

October 2017

“Ao meu Pai”

Abstract

This work is about coastal upwelling in the region of Aveiro, aiming to understand and simulate the generation of filaments during an upwelling event in the summer of 2011. This region is well-known for the formation and development of these type of hydrodynamic structures and also presents some interesting topographic features, such as, the canyon of Aveiro.

The main issue addressed is whether the existence of the Western Iberian Buoyant Plume (WIBP) due to river discharges, affects the formation of the so-called Aveiro filament.

To verify the influence of the plume on the filament formation, numerical simulations were performed using the hydrodynamic 3D model MOHID, in two distinct scenarios. In the first scenario, the model was initialized with the known values of temperature and salinity, whereas in the second scenario the coastal fresher water was replaced by saltwater with a salinity equal to 35.9 psu.

The results obtained for the first scenario show a good correlation with the ARGO buoys, and the MOHID model even performed better than the MERCATOR model. Comparing both scenarios, the main conclusion of this work is that the plume, considering only the contribution of the salinity, does not affect the filament extension but rather its direction, since there is a southward displacement. In terms of filament extension, MOHID model was compared with an analytical model, the Lentz's model. The comparison confirmed that the replacement of coastal fresher water by saltwater does not affect the filament extension, which is about 150 km in both cases. However, Lentz's model shows that without the salinity signature of the WIBP the buoyant plume reaches a distance of 122 km, while without the temperature signature the offshore distance is 127 km. These reductions in the filament extension were not observed with the MOHID model.

Keywords: costal upwelling, MOHID, ocean circulation, filaments, Western Iberian Buoyant Plume

Resumo

Este trabalho é sobre o afloramento costeiro na região de Aveiro, com o objetivo de compreender e simular a geração de filamentos durante um evento de afloramento costeiro no verão de 2011. Esta região é conhecida pela formação e desenvolvimento desse tipo de estruturas hidrodinâmicas e também apresenta algumas características topográficas interessantes, como o canhão de Aveiro.

O principal problema abordado é saber se a existência da pluma na costa ocidental ibérica (WIBP) proveniente das descargas dos rios, afeta a formação do chamado filamento de Aveiro.

Para verificar a influência da pluma na formação do filamento, realizaram-se simulações numéricas com o modelo 3D hidrodinâmico MOHID, em dois cenários distintos. No primeiro cenário, o modelo foi inicializado com os valores conhecidos de temperatura e salinidade, enquanto que no segundo cenário a água menos salina junto à costa foi substituída por água com salinidade igual a 35,9 psu.

Os resultados obtidos para o primeiro cenário mostram uma boa correlação com as observações obtidas nas bóias ARGO, obtendo-se melhores resultados com o modelo MOHID do que com o modelo MERCATOR. Comparando ambos os cenários, a principal conclusão deste trabalho é que a pluma, considerando apenas a contribuição da salinidade, não afeta a extensão do filamento, mas sim a sua direção, uma vez que existe um deslocamento para sul. Em termos de extensão de filamento, comparou-se o modelo MOHID com um modelo analítico, o modelo de Lentz. Em ambos os casos, o transporte offshore da pluma é aproximadamente igual a 150 km. No entanto, o modelo de Lentz mostra que, sem a assinatura de salinidade da WIBP, a pluma atinge uma distância de 122 km, enquanto que, sem a assinatura de temperaura, a distância atingida é de 127 km. Esta redução na extensão do filamento não foi observada nos resultados do MOHID.

Palavras-chave: afloramento costeiro, MOHID, circulação oceânica, filamentos de afloramento costeiro, pluma dos rios na costa ocidental ibérica.

Acknowledgments

Em primeiro lugar, gostaria de agradecer ao Prof. Dr. Aires dos Santos e à Profª. Drª Lígia Pinto, por toda a orientação prestada, pela exigência e motivação que me transmitiram, sendo que de todo importante salientar toda a disponibilidade desde o início do desenvolvimento da dissertação. Um grande obrigado.

Agradeço também ao Dr. Paulo Oliveira por ter dado a sua contribuição não só para o tema da dissertação a desenvolver como também quais as características que poderiam ser mais importantes reter e analisar desde o inicio do desenvolvimento da dissertação.

Quero agradecer também ao João Sobrinho e ao Francisco Campuzano do MARETEC – Instituto Superior Técnico, pela disponibilidade e pela ajuda prestada no decorrer deste projecto que, sem esta preciosa ajuda, por vezes teria sido mais complicado resolver certas dúvidas da minha parte.

Quero deixar um agradecimento muito especial à minha mãe e ao meu irmão todo o carinho e motivação que me deram ao longo de todo o meu percurso académico.

Agradeço à namorada por todo o apoio, disponibilidade e carinho e por me ter ajudado a aceitar cada desafio tendo em conta sempre o lado positivo, permitindo-me não desanimar durante o decorrer deste trabalho.

Agradeço a todos os meus amigos, com especial destaque para o Admir Rosa, o Pedro Luz e o Carlos Rodrigues, por todo o apoio, disponibilidade e atenção que me prestaram para me encorajar nas melhores formas de encarar os desafios que foram surgindo ao longo deste trabalho.

Agradeço a todos os meus colegas do BackOffice da campanha EDP Comercial, pertencente à empresa Contact – Criamos Ligações, na qual trabalhei durante o meu período de mestrado, por me terem de motivado e encorajado a obter bons resultados durante o mesmo. Não esquecendo também, o facto de terem sido compreensivos em dias menos bons, estes que, por vezes existiram em alturas mais críticas.

Table of contents

Index of figures

List of acronyms

AID – Alternating direction implicit

CTZs - Coastal Transition Zones

ENAWsp – Eastern North Atlantic Water of subpolar origin

ENAWst – Eastern North Atlantic Water of subtropical origin

GOTM – General ocean turbulence model

IPC - Iberian Poleward Current

MM5 – Mesoscale atmospheric Model

MOHID - Hydrodynamic model

NAO - North Atlantic Oscillation

OBC – Open Boundary Conditions

PC – Portugal Current

PCC -Portugal Costal Current

PCOMS – Portuguese Coast Operational Modelling system

SST – Sea Surface Temperature (^{o}C)

WIUE - Western Iberia Upwelling Ecosystem

List of symbols

α	Coefficient of thermal expansion
β	Coefficient of saline contraction
η	Free Surface Level (m)
ρ	Density (kg/m^3)
ρ_0	Reference Density (kg/m^3)
ρ_a	Density of the air (kg/m^3)
τ_y	Wind stress along y direction (Pa)
A_e	Entrainment area
C_d	Drag coefficient
U_e	Ekman velocities
K_H	Horizontal turbulent diffusivity (m^2/s)
K_v	Vertical turbulent diffusivity (m^2/s)
Ri_c	Richardson number
$\|V\|$	wind velocity modulus (m/s)
V_y	wind velocity along y direction (m/s)
W_e	Rossby deformation radius
$\tilde{h}_o$	Normalized thickness at the offshore edge of the plume
p_{atm}	Atmospheric Pressure (Pa)
v_H	Horizontal turbulent viscosity (m^2/s)
v_v	Vertical turbulent viscosity (m^2/s)
A	Generic property
S	Salinity (PSU)
T	Temperature (^{o}C)
d	depth of the Ekman layer (10 m)
Fs	Sources
Ft	Sinks

f Coriolis parameter

p Pressure (Pa)

u Horizontal Velocity in x (m/s)

v Horizontal Velocity in y (m/s)

w Vertical Velocity in z (m/s)

1. Introduction

1.1. Context

In the last decades, studies have highlighted the importance of the temporal and spatial structure of upwelling to understand the high levels of productivity of coastal upwelling systems. The high levels of productivity in upwelling regions explains due to the vertical transport of nutrients to the photic layer (Coelho et al. 1999). The upwelled water is colder than surface water, more saline and rich in nutrients, such as nitrate, phosphate, and silicate resulting from the decomposition of organic material sinking from the surface. These nutrients feed phytoplankton in the mixed layer, which is eaten by zooplankton, which in turn is eaten by small fish and so forth. Therefore, marine ecosystems in the eastern regions of the oceans are quite productive, providing the food needs of large quantities of plankton and large fish populations, such as sardines and anchovies, as well as mammals. As a result, upwelling regions coincide with the world's major fisheries regions. These conditions are paramount for the development of sardine, since phytoplankton is an important component of their diet (Garrido et al. 2006).

The summer upwelling events along the Portuguese coast which have been studied in the last decades (Fiúza et al. 1982; Haynes et al.1993; Peliz et al., 2002) have shown that the sea surface temperature (SST) and chlorophyll-a ([Chl-a]) patterns are similar to those observed in other coastal upwelling regions. They are characterized by cold pigment-rich filament structures extending offshore, as well as eddies penetrated along these upwelling fronts, which enhance primary production.

The scientific interest in the upwelling systems continues until today since they are highly sensitive to the global climate change. The North Atlantic Oscillation (NAO), which is the principal climate influence at middle and high latitudes of the North Atlantic Ocean (Hurrell, Kushnir, and Ottersen 2003), induces changes in SST (Visbeck et al. 2003), upwelling patterns (Borges et al. 2003) and marine trophic levels (Drinkwater et al. 2003) in the North East Atlantic Ocean.

Another important aspect that has been studied, but practically absent in scientific literature, is the influence of terrestrial freshwater sources in the formation of filaments. In particular, for the region of Aveiro, located in the NW of the Portuguese coast, the major discharges are from rivers Douro, Minho and Mondego with the Galician Rias having a minor contribution. These freshwaters originate a low salinity water lens that extends along the Portuguese west coast as a buoyant plume, present all year around. It constitutes a recurrent pattern in most hydrographic data of the region, being known as the WIBP. Researchers don't know exactly how the WIBP interacts with coastal upwelling in the northern Iberian coast. It is a challenge issue, which has not yet been addressed numerically.

This work leads to a better contribution in order to understand the knowledge about the processes that influences the development of the upwelling filaments in the Portuguese coast.

1.2. Objectives

The present dissertation has two main objectives. Firstly, the study of the interaction of the upwelling jet with counter-flows near the Aveiro region, during the Summer of 2011.

The second objective consists in the analysis of the contribution of the freshwaters from the WIBP, its role in the upwelling process and in the formation and development of upwelling filaments.

1.3. General methodology

The methodology used to achieve the objectives, consisted in three main steps which are:

- 1st: analysis of the satellite images available for the study area in order to identify the period with upwelling of filaments;
- 2nd: implementation of a 3D hydrodynamic model (MOHID Water Modeling System) that allows the simulation of the physical processes.
- 3rd: Implementation of two scenarios: the first one consists in simulations without any changes in the initial conditions and the second one, was modified the initial salinity near the coast, to assess the influence of the WIBP in the filaments formation. The results of the MOHID model were compared between the two scenarios.

1.4. Thesis structure

This dissertation thesis consists in five chapters (Figure 1):

Chapter 1 is an introduction that describes the framework of this thesis, the definition of the research objectives and the structure of the present work.

Chapter 2 is mainly devoted on the state of the art. Some of the most relevant papers on coastal upwelling are mentioned, with special emphasis on these related to the region of Aveiro. Also, the contribution of the freshwater form the WIBP is analysed, in what concerns upwelling and the formation and development of upwelling filaments.

Chapter 3 presents the methodology to identify the upwelling filaments and the mathematical model applied in the numerical simulations.

Chapter 4 concerns the validation and the statistical analysis for the numerical model applied.

Chapter 5 concerns the results and their analysis.

Finally, **chapter 6** devoted to the conclusions and future work.

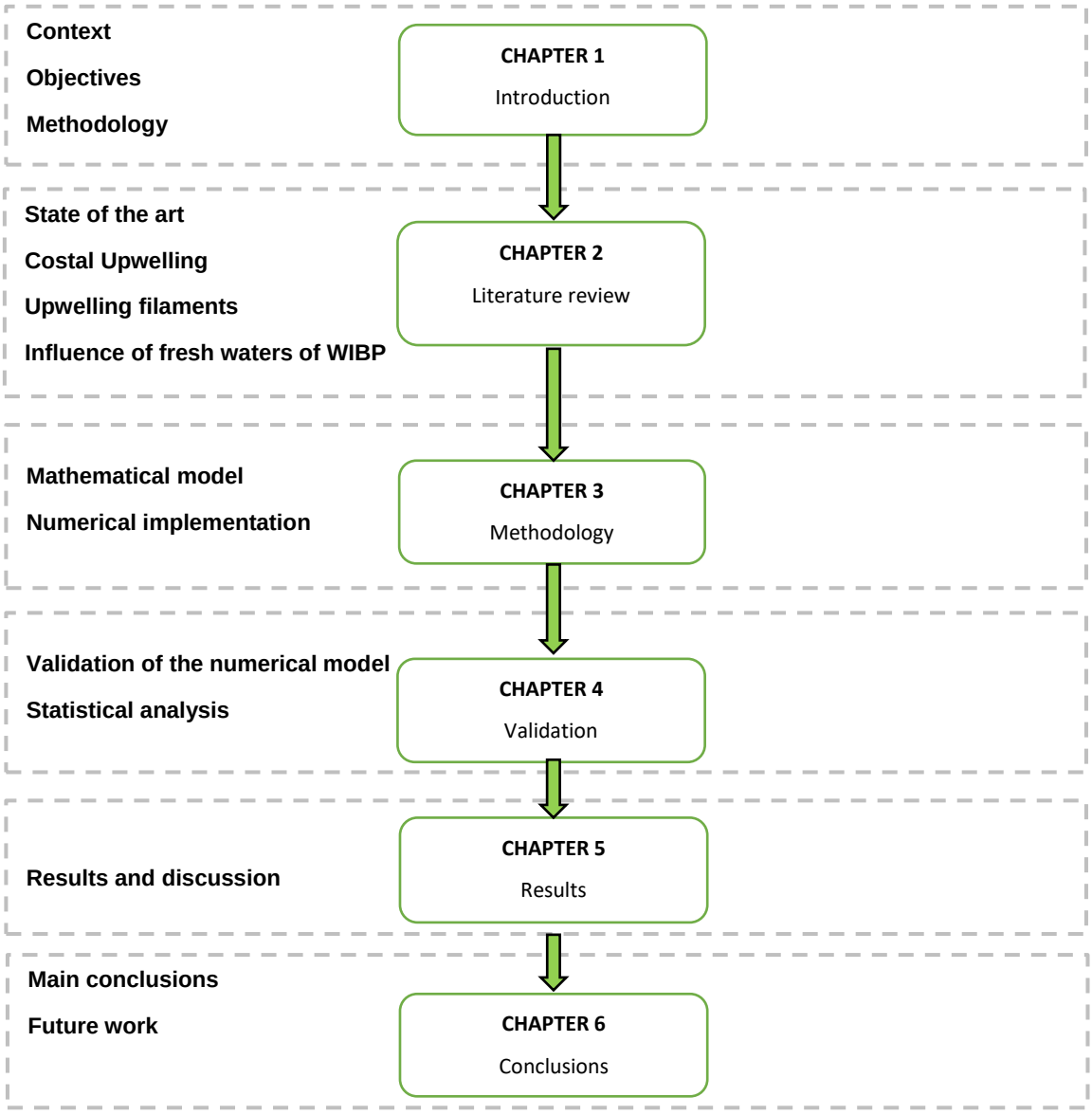

Figure 1 - Structure of master thesis

2. Literature Review

In this chapter, the basic concepts of coastal upwelling will be addressed as well as the state of the art regarding this subject.

2.1. Description of the study area

2.1.1. West Iberian

The Western Iberia Upwelling Ecosystem (WIUE) is part of the Canary Current Upwelling System (Figure 2), which extends from the northern Iberian Peninsula at 43°N to the south of Senegal, at approximately 10ºN. This upwelling system is one of the world's major Eastern Boundary Currents a very productive ecosystem and an active fisheries region.

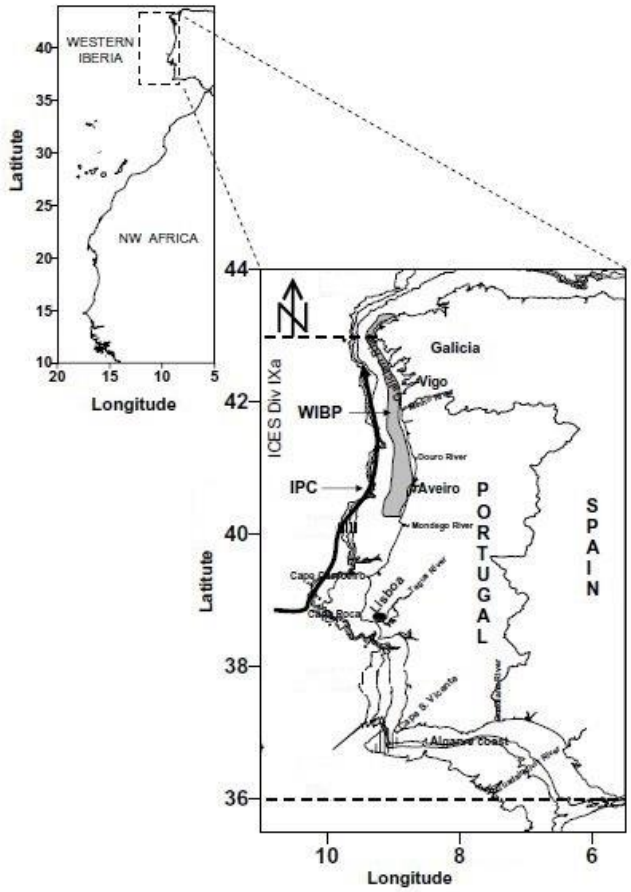

Figure 2 - The Western Iberia Upwelling Ecosystem (WIUE). The small map represents the whole Canary Current Upwelling System, in which the location of the WIUE is represented by the dashed rectangle. The main oceanographic features referred in the text are represented, namely the Western Iberia Buoyant Plume (WIBP) and the Iberian Poleward Current (IPC).(Santos et al. 2007).

The WIUE are comparable to other four principles Eastern Boundary Currents like the Canarian current, located between the northwest of the Iberian Peninsula and the northwest of Africa (Senegal coast), the current of Benguela in the southwest of Africa, the current of California, in the West of North America, and the current of Peru (or Humboldt), to the West of South America.

The main oceanographic features along the Western Iberia coast are the seasonal upwelling of nutrient-rich waters in summer, the WIBP originated from river discharge and observed all year round (Alvaro Peliz, Rosa, Santos, & Pissarra, 2002), the Iberian Poleward Current (IPC) and its associated mesoscale structures, and the Portugal Current.

Observations made in the coastal regions of California and Iberia (Haynes et al. 1993) show that the basic current regimes are similar and closely related to the large-scale wind climatology associated with subtropical gyres.

2.1.2. Study area

The NW Portuguese Coast is characterized by a continental shelf with widths of the order of 30 kilometers, where hydrodynamics is influenced by the wind, tide and density gradients. The meridional density gradient is responsible for the slope current, but there are also zonal density gradients due to the presence of several estuaries along the coast (Figure 3). The flow generated by these forcings is also influenced by the Coriolis force generating gradients of sea level that also contribute to currents.

In this study the observation area extends from near shore of Aveiro region to approximately 12^{o}W, between latitudes 40^{o}N and 41^{o}N (green lines in Figure 3).

In this region, the shelf break is located at the 200m isobath. This isobath defines the beginning of the Aveiro Canyon, where the slope gets very steep just in a few kilometers. In the north and the southern edges of this canyon there is a persistent recurrent filament activity during upwelling events (Haynes et al.,1993).

Figure 3 - Geography of the Western Iberian Ecosystem, showing the main features referred to in the text. The 200m bathymetric contour, that roughly delimits the continental shelf, is represented. From north to south: CO, Cape Ortegal; CF, Cape Finisterre; OC, Oporto Canyon; AC, Aveiro Canyon; NC, Nazaré Canyon; CC, Cape Carvoeiro; CR, Cape Roca; CE, Cape Espichel; SB, Setúbal Bay; CS, Cape Sines; CSV, Cape São Vicente; PC, Portimão Canyon; CSM, Cape Santa Maria (Adapted from: Relvas et al. 2007).

Accoding to Woster and Reid (1963) part of the variability of circulation in the study area results from the seasonal alternation of prevailing favourable to upwelling and downwelling events in spring–summer and autumn–winter, respectively. However, much of the variability of atmospheric forcing in the area is concentrated in scales shorter than seasonal, with a typical time scale of 3–14 days.

2.1.3. Hydrodynamic characterization

As was mentioned before, the Iberian Peninsula Upwelling System if often associated to one of the four wind-driven Eastern Boundary Upwelling Systems, the well-known Canary-Iberian upwelling.

However, there is an important difference between the Canary and Iberian areas in the Canary region, quasi-constant trade winds favor upwelling all year round, whereas in the Iberian region there is a strong seasonality mainly due to the annual cycle of the atmospheric circulation.

The Iberian Poleward Current (IPC)

The slope current, a poleward flow along the Iberian coast with its core at the upper continental is a regular pattern all year round (Coelho et al. 1999). In the winter, the southerly wind reinforces it, whereas during the upwelling season, its existence is still a subject of ongoing research.

Many authors have provided evidence for a poleward flow along European slopes (Frouin et al. 1990; Haynes and Barton 1990; Pingree and Le Cann 1990). Very similar poleward flows have been described in other eastern boundary regions such as the California Current System (CCS) and the Leeuwin current at the West Coast of Australia.

According to Frouin et al., (1990) the IPC observed along the west coast of the Iberian Peninsula is characterized by a transport of warm and salty water with velocities between 0.2 and 0.3 m/s. The associated transports are $300x10^3$ m^3/s at about 38°N and $500\text{-}700x10^3$ m^3/s around 41°N. The transport values show a poleward intensification of the slope current, which is also a characteristic of the poleward currents at the eastern boundaries.

More recently, Peliz et al. (2005) characterized the poleward current by a tilt down of the isopycnics towards the coast in the upper 200 m, in an across-shore distance of about 40 km. The poleward current system is rich in mesoscale features, like instabilities of the flow and eddy interactions.

However, the poleward flow during summer allows the thermal signature of the light water, because the surface layer is strongly modified by heat fluxes, and the upwelling event in the frontal zone at the slope region, giving origin to the formation of filaments, tend to mask the thermal contrast typical of winter poleward flow.

Nevertheless, Peliz et al. (2002) observed the tendency of the poleward flow going offshore during the summer. However, Peliz et al. (2005) hypothesize that the poleward current does not reverse completely but that the core of the flow is moved offshore and that the slope zone is occupied by dominantly equatorward current. Poleward flows, are sometimes dominant features of eastern boundary upwelling systems, and have a key role in the onset of harmful algal blooms with significant economic repercussions for local fisheries (Relvas et al. 2007). These flows also are instrumental in forming convergence zones over the shelf-break off the NW Iberia, which have an ecological importance in the retention and/or poleward transport of the phytoplankton.

The Portugal Current (PC), a south-west surface drift offshore, is established and is usually associated with a coastal jet flowing equatorward (Pelíz et al. 2002). In addition, the IPC is observed at many periods of the year but intensified in non-upwelling season, i.e. during winter (Peliz et al. 2005).

Circulation on Aveiro region

A study realized by Fraga (1992) identified two types of central waters off Western Iberia: Eastern North Atlantic Water of subpolar origin (ENAWsp) and Eastern North Atlantic Water of subtropical origin (ENAWst). The ENAWsp is related with the Subpolar Mode water, which forms due to deep convection during Winter in the Eastern North Atlantic, at 46ºN (McCartney 1992). The ENAWst water is formed in the north of the Azores Current at approximately 35ºN and is advected northwestward, creating with the ENAWsp a subsurface font characterized by intense convergence in the proximity of Cape Finisterre between 42ºN and 44ºN (Fraga, 1992). Another study done by Paillet (1996), proves that the ENAWst is the main source of upwelled waters at the Iberian coast.

Figure 4 presents the conceptual model of Peliz et al. (2002), showing the major features of ocean circulation, offshore of Aveiro, during the upwelling season. The equatorward upwelling jets create a double-frontal system. The main one is located off the 100m isobath and the second one is located at the inner-shelf region. The figure also shows the PC (yellow colour), as well as an anticyclonic eddy that results from the interaction between the IPC and the upwelling jet. The hypothesis formulated in Peliz et al. (2002), is that both the anticyclonic eddy and the WIBP contribute to the offshore propagation of the upwelling filament located at the latitude of Aveiro.

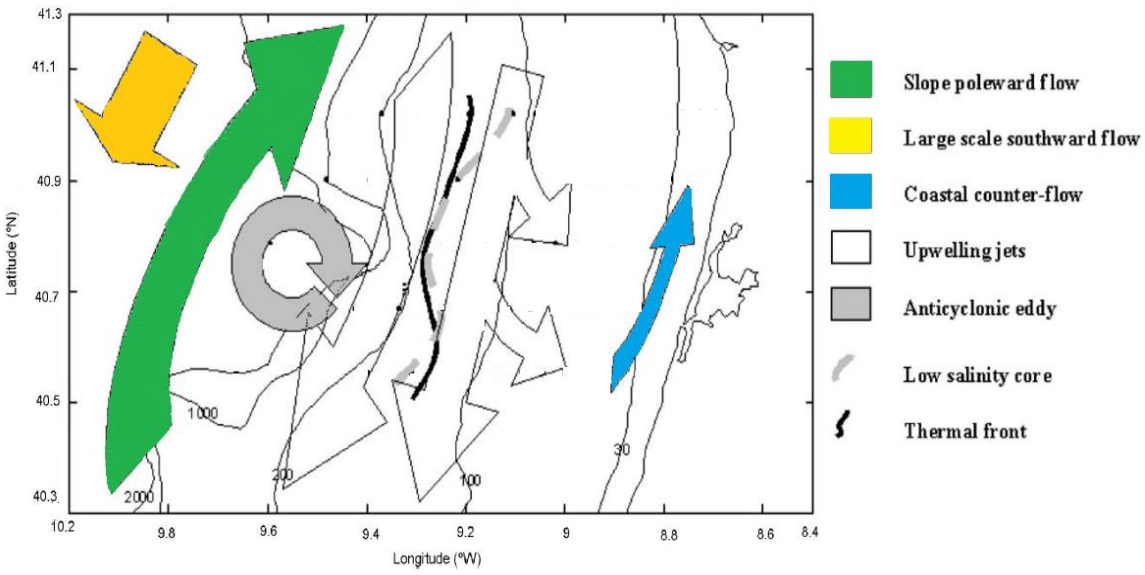

Figure 4 - Conceptual model of the circulation near Aveiro. Adapted from Peliz et al. (2002)

2.2. Ekman theory and costal upwelling

In oceanography and climatology, one of the most important theory is the one which was presented by Ekman (1905), known as Ekman Theory. This theory is one of the most important theory in oceanography and climatology and explains the existence of coastal divergences or convergences, i.e., coastal upwelling or downwelling.

As the wind exerts frictional forces over the ocean surface, it creates movement in the most superficial water layer, which in theory is deflected to the right (Northern Hemisphere) about 45° to the direction of the wind, due to the Coriolis effect. This effect propagates vertically in the water column, exhibiting a deflection in the same direction but whose angle increases and whose speed decreases downwards, due to the friction, until reaching the depth of 50-100 m. This limit is considered to be the thickness of the mixed layer where all properties (e.g. salinity and temperature) are almost constant due to the influence of the wind. If the vertical velocity is plotted in the vertical, it describes a spiral known as the Ekman spiral (Figure 5).

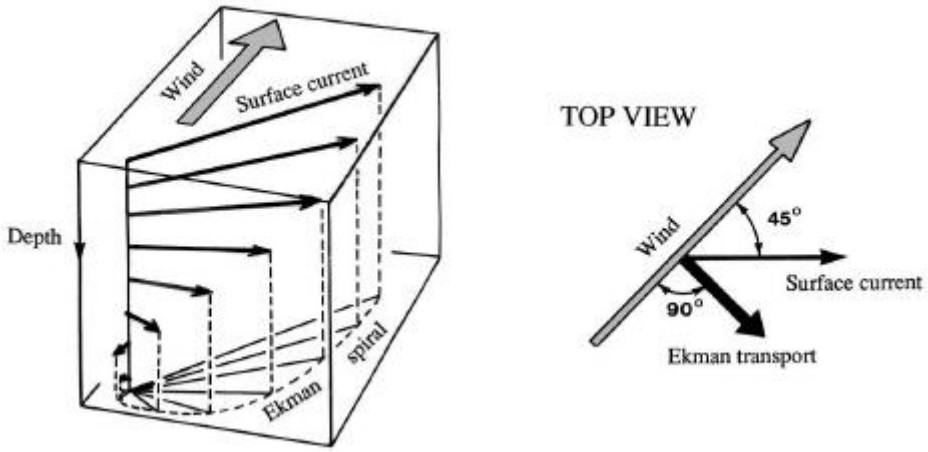

Figure 5 - Ekman Spiral. The figure represents a draw for the Northern Hemisphere (f>0), the deflection being to the right of the surface stress (Cushman-Roisin, 2008)

The Ekman Spiral in Figure 5 shows that the average movement in the mixed layer is at 90° to the right (left) of the surface of wind direction in the Northern Hemisphere (Southern Hemisphere). This net transport is called the **Ekman transport**. In this case of the Portuguese coast oriented in the North-South direction, for the northerly wind the Ekman transport is in the offshore direction and upwelling occurs (Figure 6).

Figure 6 - Upwelling process (source: Cordell Bank National Marine Sanctuary).

Globally, there are four major currents associated with coastal upwelling. They correspond to the eastern branch of the anticyclonic circulation in the subtropical gyres (Figure 7). In the Atlantic Ocean, we have the Canaries current (red region in A) and the Benguela Current (red region in B), while in the Pacific Ocean we have the California current (red region in C) and the Peru (or Humboldt) current (red region in D).

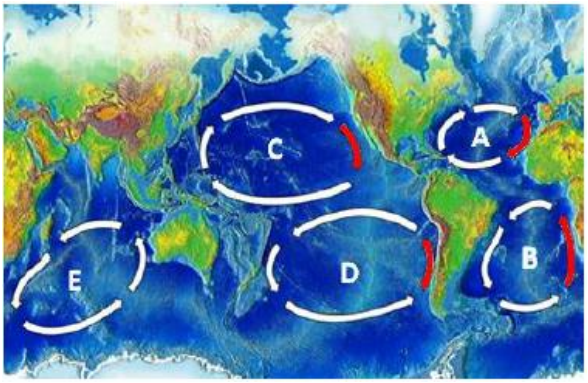

Figure 7 - Geographical location of the main oceanic subtropical gyres: subtropical gyre of the North Atlantic (A), subtropical gyre of the South Atlantic (B), subtropical gyre of the North Pacific (C), subtropical gyre of the South Pacific (D), subtropical gyre of the Indian ocean (E). The red arrows represent the major ocean currents associated with coastal upwelling. Image adapted from NOAA.

2.2.1. Costal upwelling in Portuguese west coast

The coastal upwelling events exchanges water and biogeochemical properties with the offshore regions through the complex and highly dynamical Coastal Transition Zones, the core of many multidisciplinary studies in the last two decades. Most of the current studies about coastal upwelling in Western Iberia were done using satellite imagery and *in situ* data. However, some *in situ* studies that have been conducted during upwelling periods present a lack of resolution.

Coastal upwelling and the outcrop of the thermocline, originates a frontal system, which is prone to the formation of several instabilities. In the onshore region, another type of front can be formed related to gradients of salinity, when the freshwater from rivers meets the salty oceanic water. There is a second front at the inner-shelf between equatorward upwelling jet and the coastal counter-flow related to the WIBP. The slope of the isopycnics associated with the lighter water from WIBP, may explain this northward counter-flow.

Studies done by Frouin et al. (1990); Haynes & Barton, (1990) prove that when upwelling does not occur the costal circulation off Western Iberia is predominantly northward. These northward circulation is partially driven by meridional alongshore density gradients and assumes a character of a poleward jet transporting higher salinity and warmer (subtropical) waters over the upper slope and shelf break.

Pulses of weak to moderate upwelling disrupt stratification and bring nutrients into the photic zone allowing phytoplankton growth on the inshore side of a well-developed thermal front, whereas oceanic waters are poor in phytoplankton due to nutrient depletion in the surface layer.

Fiúza et al., (1982) analysed the wind regime along the Portuguese using monthly climatological averages between 1931-1960 (30 years) and concluded that coastal upwelling occurs from July to September in consequence of the increase in the intensity and steadiness of northerly winds in June, July and August. This can be explained by the northward displacement of the Azores high and Iceland low during the summer, as well as he presence of an Iberian low during the same period.

For a southerly wind, more frequent on the Portuguese coast during the winter, the joint effect of the wind forcing, density and freshwater discharges generates a surface northward current. However, episodes of winter upwelling associated with a northerly wind, have also been observed. These events might be related to the NAO and may have important consequences or the survival of sardine larvae during the spawning season (Santos, Nogueira, and Martins 2005).

By the end of summer (September–October), there is a shift in the wind regime to downwelling favourable south westerlies, along with the onset of the relatively warm and saline Iberian Poleward Current (IPC) over the slope (Haynes et al. 1993; Peliz et al. 2005; Relvas et al. 2007).

According to Bakun et al. (2009), it is during the spring-summer months that there is a general increase in the trends of coastal upwelling in subtropical latitudes. Further, of along the Iberian Peninsula, they identified a consistent pattern of increased wind intensity in areas subjected to low-pressure thermal cell formations during the warm-up periods of the year.

It is known that during the summer in the interior of the Iberian Peninsula, when the incident solar radiation reaches maximum values on its arid and semi-arid surface, a thermal low is formed. In addition, the difference in thermal capacity between land and water originates

mesoscale circulations known as sea breezes. These zonal gradients of pressure interacting with the Coriolis force reinforce the northerly wind.

Hoinka and Castro (2003) concluded that during the months of June, July and August the likelihood of this thermal lows is 0.35 - 0.45, with a maximum intensity at 18 UTC, located near 40.5ºN and 4.0ºW. This northerly wind regime is characterized by an increase of the wind intensity throughout the day, reaching maximum values at the end of the afternoon (corresponding to the maximum intensity of the thermal low). This intensification along the Iberian West coast has a direct impact on coastal upwelling.

2.2.3. Upwelling filaments

Coastal filaments are relatively narrow (typical widths of a few tens of kilometers) and shallow (usually no deeper than 150 m) stretching offshore up to several hundred kilometers from the coast. The core of a filament flows offshore with rather large velocities, usually between 0.25 and 0.5 m/s, and it is common to find onshore flows at both sides of the filament associated eddies. Filaments are frequently observed in all eastern boundary currents of subtropical gyres and are almost always associated with upwelling favourable conditions, therefore they contain relatively cold water of subsurface origin. Upwelling filaments intensify the exchange processes of biological properties in open ocean waters (Cravo et al. 2010), since their offshore transport is usually significantly larger than the Ekman transport (Kostianoy and Zatsepin 1996). However, there is a lack of knowledge about how the physical dynamics of the upwelling filaments affects the chemical and biological processes, which makes difficult to draw any global conclusions on their effects.

Filaments can persist even during periods when there are no upwelling favourable winds, meaning that these structures have greater inertia than the costal upwelling itself. (Castro et al. 2000).

According to Ramp et al. (1991) and Strub et al. (1991), the development of filaments may result from one or a combination of several factors: baroclinic instability of the coastal current, irregularities in coastline and bottom topography, coastal divergence caused by the wind stress, and the interaction of eddies with the coastal region.

Haynes et al. (1993), based on Sea Surface Temperature (SST) observations suggested that filaments anchored to capes are probably related to topographic forcing leading to the separation of the upwelling jet, whereas in areas with smooth coastlines and bathymetry, they are probably related to the development of frontal instabilities.

Lars and Shi, (1999) have investigated the generation of such structures with reduced gravity models and concluded that "*they do not depend on coastline or bathymetric irregularities to start developing, but shelf/slope topographic forcing is an important mechanism for the anchoring of these mesoscale structures".*

In the Western Iberia, the intensity and persistence of coastal upwelling conditions in spring and summer, promotes the transport of nutrients like Nitrate (NO_3^-) to the euphotic zone, as well as phytoplankton growth (Nogueira, Pérez, and Ríos 1997) which sustains the high zooplankton biomass observed from early spring to late autumn, when north-easterly winds prevail along the western Iberian coast. During early spring, when there is enough wind and a weak thermal stratification for phytoplankton blooms, they are advected from the coast and can appear on the oceanic side of a poorly developed upwelling front. Under these conditions, chlorophyll-a maxima are often found in an area of convergence or retention formed by the IPC, which serves as a barrier to shelf ocean exchange of upwelled waters (Santos et al., 2004).

When equatorward winds start to prevail (late spring/early summer), a narrow band of cold water of relatively uniform width is observed along the coast, and small scale (20–30 km) perturbations are usually seen along the thermal front. Approximately one month after the beginning of upwelling favourable winds, major filament structures start to develop gradually into larger filaments, associated with offshore currents reaching 0.5 m/s, leading to the classical picture of what is usually called ''fully developed upwelling'' where several cold-water filaments are seen to extend more than 200 km offshore.

In the past decades, satellite-derived SST maps were used to verify the upwelling patterns in a certain region. The filaments develop seaward from the meandered upwelling front and leave a clear signature in SST satellite imagery.

According to Haynes et al. (1993), the observations of filaments in the Iberian coast become more exhaustive in the early 1980s, with the identification of cold water filaments in satellite imagery. The same paper refers that the filaments become common around the start of July, reach their maximum frequency in mid-September and then decline in abundance to become relatively rare by the end of October.

A sequence of satellite images in 1982 (Figure 8), shows the development of the filaments structures in that period.

Three periods were analysed:

- On August 9, incipient filaments were evident as bulges in the upwelling front at 42ºN 30'N, 41º 10'N, and 40º 20'N (Figure 8 on the left);
- By August 20, the cold-water mass extended offshore about 100 km, (Figure 8 in the middle);

- The offshore progress of these filaments continued until the beginning of September when the “nose” of the filament “anchored” at 42ºN reached approximately 200km (Figure 8 on the right).

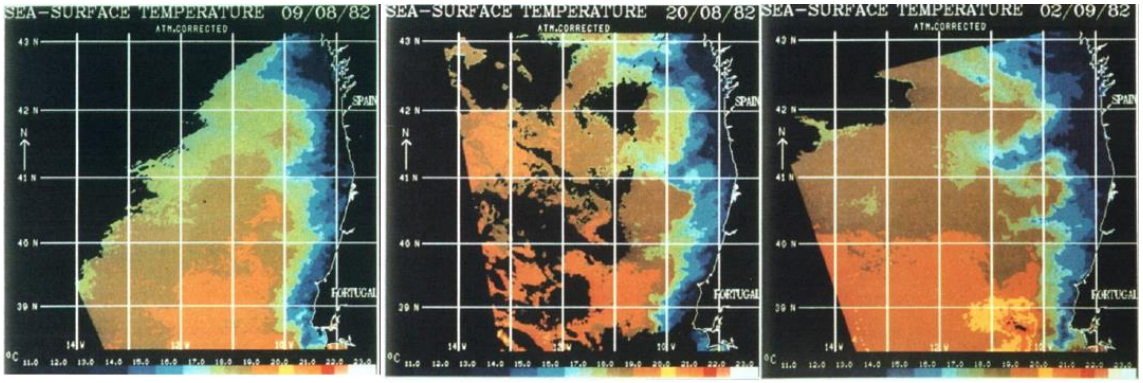

Figure 8 - Sequence of satellite images from 1982. The picture on the left shows the beginning of the formation of filaments. In the middle, the filaments have an extension of approximately 100km and on the right they are fully developed and extend 200 km from the coast. (Haynes et al., 1993).

More recently, Cravo et al. (2010) studied an upwelling filament off southwest Iberia and found that it carried large concentration of chlorophyll-a as well as nutrient offshore the coastal upwelling front. In the same paper a review of the existing bibliography in the North Atlantic showed that, large amounts of nutrients and plankton are exported towards the open ocean through these structures. They reported the existence of relatively high levels of nutrients at the base of the filament. Nutrient concentrations decrease in the offshore direction and become irrelevant at the offshore extreme of the filament. These characteristics indicate that nutrients are being utilized as the water parcels move offshore, and suggest that the direct export of nutrients by the filaments to the open ocean may be relatively small, at least compared with the export of organic matter. The regeneration of exported organic matter, however, causes an indirect export of both nutrients and dissolved organic carbon, reflected in a high correlation between these quantities (Perez et al. 2001).

2.2.4. Influence of terrestrial freshwater sources

Another key aspect about upwelling events almost neglected in scientific literature, is the influence of terrestrial freshwater sources in the costal zones due to river runoff. A significant amount of freshwater is discharged all year round to the narrow Iberian shelf by several rivers.

The river runoff is mainly dependent on precipitation, therefore it changes seasonally being higher in the winter than in summer. Nevertheless, in the North coast of Portugal the major

discharges are from rivers, Douro, Minho and also from the Galician Rias, as shown in Figure 9, that have a relevant contribution to the WIBP.

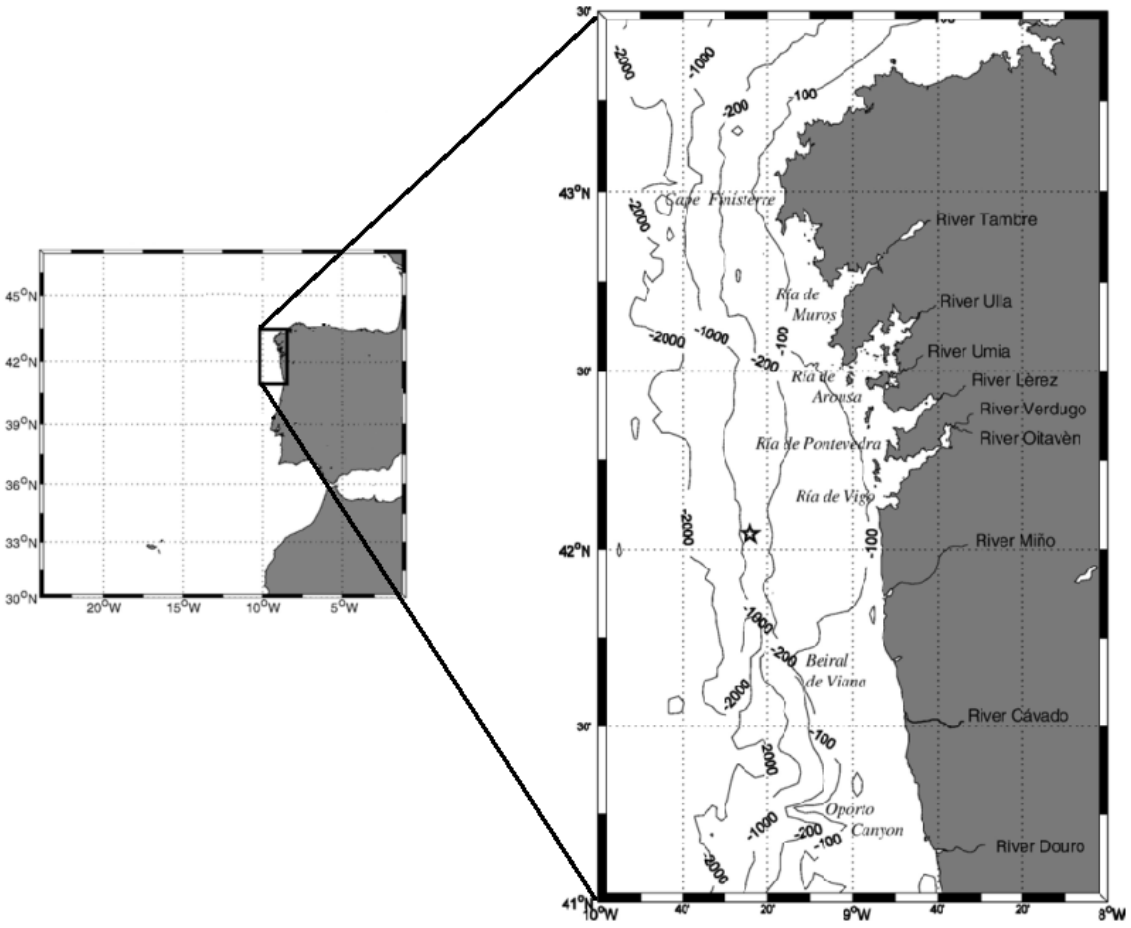

Figure 9 - Rivers that contributes to fed WIBP (Otero, Ruiz-villarreal, and Peliz 2008).

According to Peliz et al., (2002), the accumulated river run-off generates a buoyant plume that extends along the coast and is present all year around, having a strong influence on shelf circulation. The WIBP is made of low salinity water (S< 35.8 psu) from winter runoff of several rivers, mentioned above, on the North coast of Portugal and Spain (Peliz et al. 2005; Peliz et al. 2002). This plume promotes a strong stratification over the shelf that reduces the thickness of the Ekman layer and the offshore Ekman transport, creating a front along the inner-shelf associated with a northward baroclinic transport. This current, interacting with the topography and the upwelling jet, plays an important role in filament development.

The Ekman dynamics cause an offshore displacement of the plume and, in turn, the northward flow forces a poleward advection. Moreover, the several mesoscale features associated with the this current, affect both advection and mixing of the plume (Santos et al. 2004).

A study realized by Ribeiro et al. (2005) shows that the WIBP also promotes phytoplankton growth due to the retention of nutrients, being a suitable environment for larvae survival in the North of Iberia (Santos et al. 2004).

According to Fraga (1992) part of the WIBP at the mid-shelf has lower temperatures (denser) and comes into the observed area from the north, incorporated in the upwelling jet. The part of the WIBP that is warmer (lighter) is advected to the south at the inner-shelf along the coast.

Another factor likely to contribute to the retention of the plume is the vertical circulation associated with the upwelling dynamics (Figure 10b). In the case of a deep mixed layer and moderate along-shore currents, replacement of the surface waters is done from the interior layer and the vertical circulation is closed at the outer shelf through a surface convergence of the upwelled waters (Figure 10a).

Previous studies about river plumes on the northern Portuguese shelf (Ribeiro et al. 2005; Santos et al. 2004) highlight important features of the response of the system to upwelling favourable winds. They reveal the significance to the local ecosystem of the interaction between the WIBP, wind-driven currents and the outer shelf/slope circulation. The latter consists, during autumn and winter, of warm and salty waters in the IPC. The fronts, associated with the WIBP and the IPC play role in the retention and dispersion of plankton and larvae (Figure 10) (Santos et al. 2004).

The WIBP essentially provides a vertical retention mechanism, whereas the poleward current acts like a barrier to the cross-shelf Ekman transport, retaining most of the plume close to the slope and advecting it northward. In this process, a convergence zone is created where the plume is trapped and deepens, thus increasing the potential for retention as described in Figure 10.

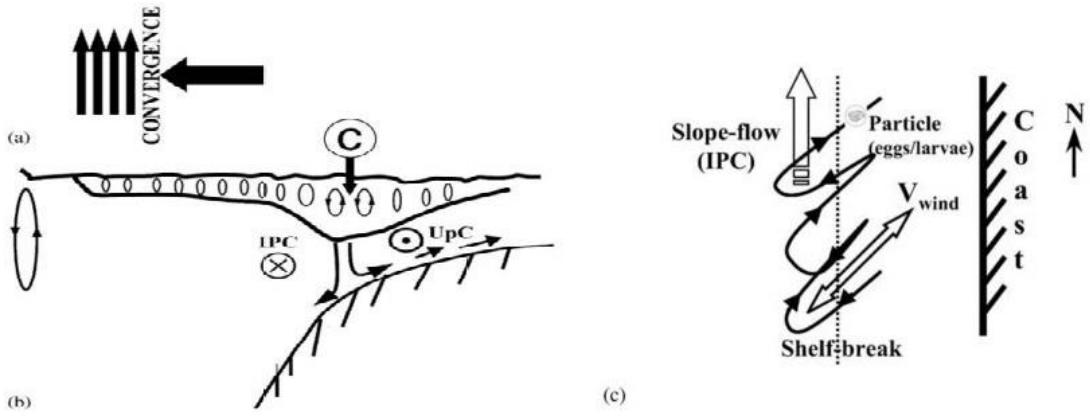

Figure 10 - Retention mechanism and poleward egg and larval drift: (a) the convergence zone mechanism; (b) the vertical retention inside the buoyant plume (IPC—Iberian Poleward Current; UpC—Upwelling current; C—Convergence zone); and (c) the horizontal retention and modulated poleward transport due to the joint effect of the poleward slope flow (IPC) and the cross shelf Ekman transport (Vwind).(Santos et al. 2004).

3. Methodology

3.1. Identification of the upwelling event and the formation of filaments

The first part of the methodology consists in the analysis of the satellite images with the aim of identifying the period in which the upwelling event occurs, as well as possible filaments near the study area, Aveiro.

The satellite images used were the ODYSSEA Sea Surface Temperature which provide daily gap-free maps of SST, at 0.02^o x 0.02^o horizontal resolution, using satellite data from both infra-red and micro-wave radiometers. These images can be observed in **5.1.**

3.2. The mathematical model

The use of numerical models can represent an appropriate tool both on process studies and on interdisciplinary integration of results. The main goal is to study the major oceanographic features, in the region of Aveiro, that characterize and may interfere with the upwelling event such as: filaments, outcrop of pycnoclines, offshore Ekman transport and the flow along the WIBP. Another important feature is the IPC, but as we already mentioned, its presence during the summer is still a subject of ongoing research.

3.2.1. Description of the model

The model used to the development of this work was MOHID water 3D (Braunschweig et al., 2002), which since its creation has been applied to various locations, with different conditions and for different purposes (e.g. Trancoso et al., 2005; Coelho et al., 1998).

This model is built through an interconnected set of modules using object-oriented programming in FORTRAN 95, as described in Decyk (Decyk et al., 1997), each module being responsible for the management of a portion of the information, summing up a total of 40 modules developed over three decades of research work. This type of programming has proven to be a very useful methodology in the development of complex algorithms, especially the ones aiming to simulate real world problems (Fernandes, 2005). MOHID uses an Arakawa type C grid (Figure 11) and a finite volume approach to calculate the velocities, the water level, and several scalar properties. In the Arakawa grid type C, the level and the scalar properties of the water are calculated at the center of the grid cells, while the velocities are calculated on the faces of each cell.

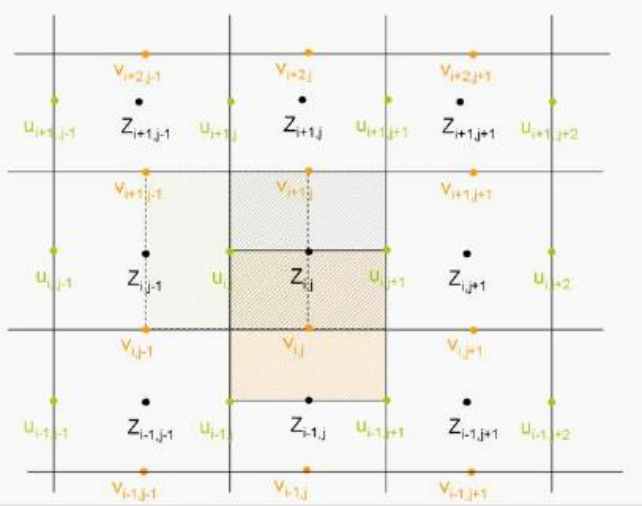

Figure 11 - Description of the Arakawara type C mesh used by Mohid indicating the location of the calculation points of the Z properties and the U and V velocities (Gomes, 2014).

3.2.2. Hydrodynamic

The hydrodynamic model MOHID used in this work (F. Martins, Neves, & Leitão, 1998; Flávio Martins, Leitão, Silva, & Neves, 2001) solves the equations of a three-dimensional flow for incompressible fluids and an equation of state relating density to salinity and temperature (Leendertsee and Liu ,1978). The equations are solved numerically using the finite volumes method, with a generic vertical discretization that allows simultaneous implementation of various types of vertical coordinates.

Hydrostatic equilibrium and the Boussinesq approximation are assumed. The model uses a alternating direction implicit (ADI) algorithm with two time levels per iteration. Vertical eddy viscosity/diffusivity was determined with a turbulence closure model selected from those available in the General Ocean Turbulence Model (GOTM), which consists of a set of turbulence-closure models (Burchard 1999).

The equations for the calculation of the average horizontal velocities are:

$$\frac{\partial u}{\partial t}+\frac{\partial(uu)}{\partial x}+\frac{\partial(uv)}{\partial y}+\frac{\partial(uw)}{\partial z}=fv-\frac{1}{\rho_0}\frac{\partial p}{\partial x}+\frac{\partial}{\partial x}\left(v_H\frac{\partial u}{\partial x}\right)+\frac{\partial}{\partial y}\left(v_H\frac{\partial u}{\partial y}\right)+\frac{\partial}{\partial z}\left(v_v\frac{\partial u}{\partial z}\right) \quad (1)$$

$$\frac{\partial v}{\partial t}+\frac{\partial(vu)}{\partial x}+\frac{\partial(vv)}{\partial y}+\frac{\partial(vw)}{\partial z}=-fu-\frac{1}{\rho_0}\frac{\partial p}{\partial y}+\frac{\partial}{\partial x}\left(v_H\frac{\partial v}{\partial x}\right)+\frac{\partial}{\partial y}\left(v_H\frac{\partial v}{\partial y}\right)+\frac{\partial}{\partial z}\left(v_v\frac{\partial v}{\partial z}\right) \quad (2)$$

Where u, v and w are the components of the velocity vector in the x, y and z directions respectively, f is the Coriolis parameter, v_H and v_v the turbulent viscosities in the horizontal and vertical directions and p is the pressure. The temporal evolution of velocities is the balance of advective transports, Coriolis force, pressure gradient and turbulent diffusion.

The turbulent viscosity is computed differently for the horizontal and vertical directions. The horizontal turbulent viscosity is defined as a constant value, dependent upon the grid resolution and a reference velocity, or as a function of horizontal velocity gradients.

After determining the horizontal velocities, the vertical velocity is calculated from the continuity equation:

$$\frac{\partial u}{\partial x}+\frac{\partial v}{\partial y}+\frac{\partial w}{\partial z}=0 \tag{3}$$

The free surface is obtained by integrating the equation of continuity over the entire water column, between the free surface elevation z= η(x, y, t) and the bottom z= - h(x, y) yielding :

$$\frac{\partial \eta}{\partial t}=-\frac{\partial}{\partial x}\int_{-h}^{\eta} u\,dz-\frac{\partial}{\partial y}\int_{-h}^{\eta} v\,dz \tag{4}$$

Where η is the surface level and h the local depth. The equation of hydrostatic pressure is:

$$\frac{\partial \mathrm{p}}{\partial \mathrm{z}}=-\rho g \tag{5}$$

where g is gravity and ρ the density. Integrating this equation in the vertical and considering that $\rho = \rho_0 + \rho'$, where ρ_0 is a constant reference density and ρ' a density perturbation, yields:

$$p(z)=p_{atm}+g\rho_0(\eta-\mathrm{z})+\mathrm{g}\int_z^{\eta}\rho' \mathrm{dz} \tag{6}$$

The equation above relates the pressure at any depth with the atmospheric pressure at the sea surface, the sea level and the anomalous density integrated between that level and the sea surface. Differentiating equation (6) yields:

$$\frac{1}{\rho_0}\frac{\partial \mathrm{p}}{\partial \mathrm{x}}=\frac{1}{\rho_0}\frac{\partial p_{atm}}{\partial \mathrm{x}}+g\ \frac{\partial \eta}{\partial \mathrm{x}}+\frac{\mathrm{g}}{\rho_0}\ \frac{\partial}{\partial \mathrm{x}}\int_z^{\eta}\rho'\,\mathrm{dz} \tag{7}$$

The total pressure gradient is the sum of the gradients of atmospheric pressure, sea surface elevation (barotropic pressure gradient) and density distribution (baroclinic pressure gradient). Regarding the density, its value is obtained from the values of salinity and temperature, using the following equation of state (Leendertsee and Liu 1978):

$$\rho=\frac{5890+38\,T-0.375\,T^2+3\,S}{1779.5+1.25\,T-0.0745\,T^2-(3.8+0.01\,T)S+0.698\,(5890+38\,T-0.375\,T^2+3\,S)} \tag{8}$$

The Hydrodynamic Model computes the advective and diffusive fluxes, the discharges of water, sediment fluxes, oxygen and heat changes with the atmosphere and sedimentation fluxes. The transport of any property A due to advection and diffusion can be described by the equation 9:

$$\frac{\partial A}{\partial t} + \frac{\partial (uA)}{\partial x} + \frac{\partial (vA)}{\partial y} + \frac{\partial (wA)}{\partial z} = \frac{\partial}{\partial x}\left(K_H \frac{\partial A}{\partial x}\right) + \frac{\partial}{\partial y}\left(K_H \frac{\partial A}{\partial y}\right) + \frac{\partial}{\partial z}\left(K_V \frac{\partial A}{\partial z}\right) + (Fs - Ft) \quad (9)$$

Where, K_H and K_v are the horizontal and vertical turbulent diffusivities of that property. The first term on the left is the partial derivative of that property with order to time, the next three terms represent the advective transport, the following three terms the diffusive transport, and $(Fs - Ft)$ represent the sources minus the sinks.

3.3. Portuguese Coast Operational Model System parametrization

The Portuguese Coast Operational Modelling System (PCOMS) is a forecast system based on the MOHID model. The modelling system consists of one nested domain covering the Iberian Atlantic coast and the Portuguese coast (Figure 12). The model was implemented using a multinest approach that allows automatic simulations in a nowcast/forecast perspective. The use of an implicit method has the advantage of numerical stability, without compromising the accuracy of results and saving simulation time, since it allows the use of a larger time step.

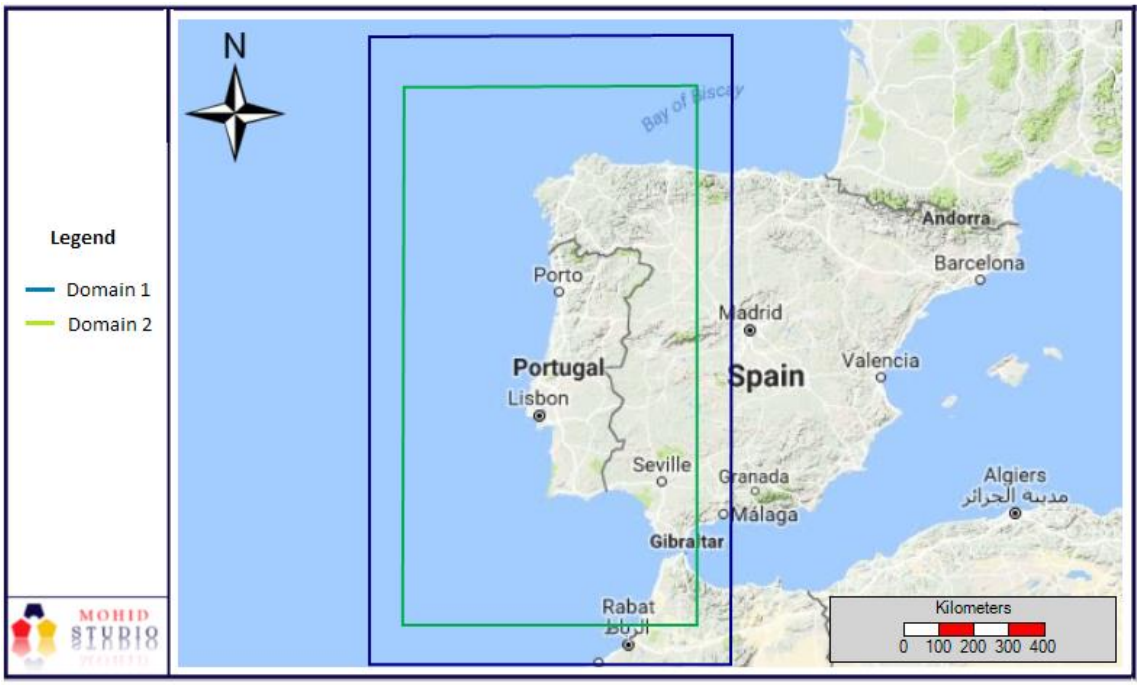

Figure 12 - PCOMS domains

3.4. Initial conditions

With the objective to observe how the WIBP affects the filament in the Aveiro region, two simulation scenarios were performed, in order to make a comparison between them. Both simulations started on 31 May 2011, with a spin up of 5 days, and ended on 30 August 2011. The first scenario consisted of performing the simulation using the PCOMS model and in the second scenario the initial conditions where changed, removing all the salinity values bellow 35.9 psu, from the Mercator file (Figure 13). Although, the literature reports a salinity value between 35.7 and 35.8, for WIBP, the value of 35.9 was chosen due to numerical stability reasons.

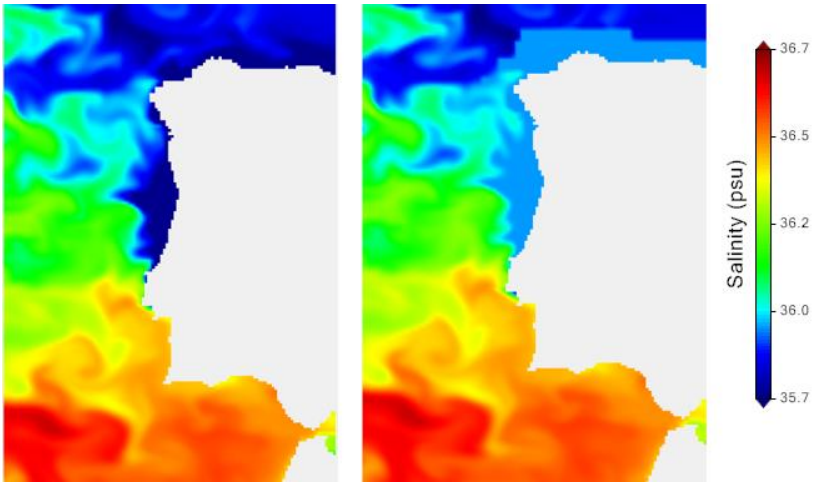

Figure 13 - Mercator initial file for scenario 1 (left) with the WIBP and for scenario 2 (right) without the WIBP.

The value assumed for the horizontal viscosity was 55 m^2/s and with a sponge value of 60000 m^2/s. The vertical turbulent viscosity was computed by the Global Ocean Turbulence Model (GOTM), which is coupled to MOHID.

3.4.1. Boundary conditions

The model requires initial conditions and boundary conditions in the land, ocean and atmosphere interfaces to solve the differential equations. In the boundaries, close to land (lateral closed boundaries), the cell faces in contact with land have null fluxes. At the free surface the model is forced by the wind surface stress, the energy and mass fluxes. At the bottom, boundary advective fluxes are null and the diffusive flux of momentum is estimated by means of a bottom stress law that depends on the near-bottom velocity.

3.4.2. Bathymetry

The bathymetry, known to be responsible for instability conditions of the model, greatly influences the water circulation and the transport of the properties in the domain. To construct the model bathymetry, it is necessary to have three elements: the grid, the bathymetric points (they should have the best resolution as possible) and the coastline.

In this work two bathymetries were used, one embedded in the other. The first and the second one was a bathymetry used in PCOMS model (described above).

Figure 14 represents the bathymetry for the first domain, used in the barotropic model with 6km resolution, forced with the Finite Element Solution (FES) 2004 global tide solution along the ocean boundary.

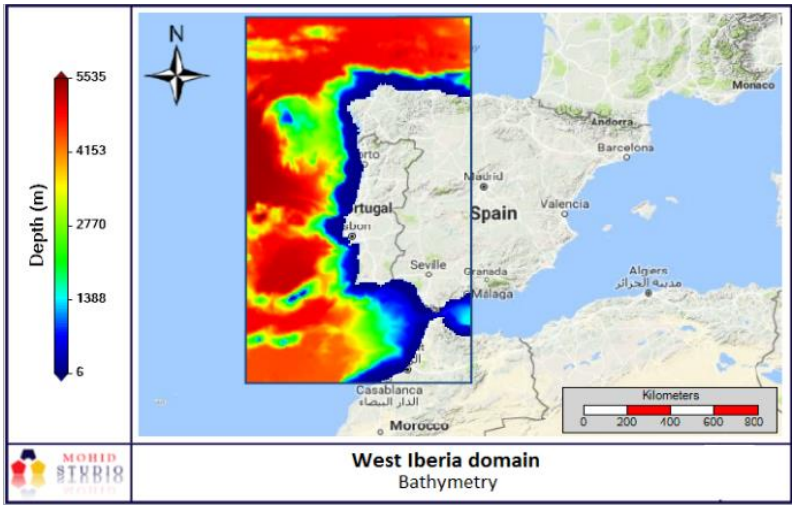

Figure 14 - West Iberia domain

The bathymetry for the second domain is presented in Figure 15. This domain is a downscaling of the Mercator-Ocean PSY2V4 North Atlantic solution that run the MOHID model in full baroclinic version with a horizontal resolution of 6km and with 50 vertical levels, 43 in Cartesian and 7 in sigma coordinates. The temperature and salinity 3D initial conditions are interpolated directly from the Mercator-Ocean fields. For the atmospheric conditions, the system is one-way coupled offline with the 9km resolution MM5 atmospheric forecast model, providing hourly results, for the west Iberian coast.

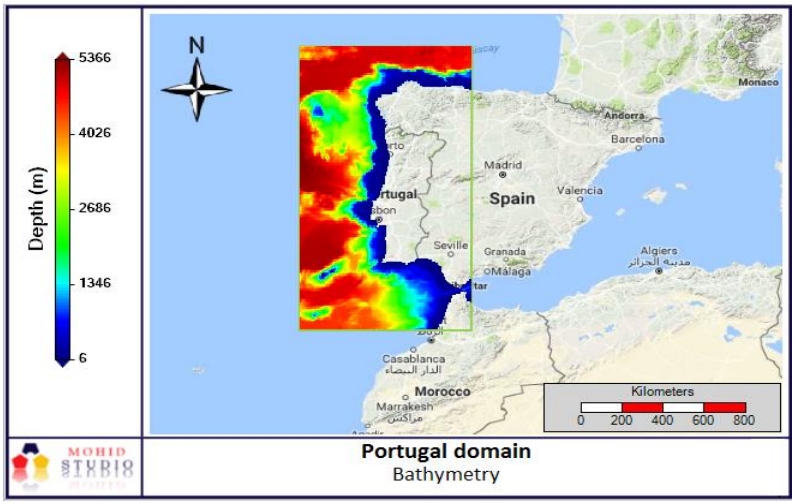

Figure 15 - Portuguese domain

3.4.3. The wind regime

The wind influences the flow by inducing a surface water velocity dependent upon the wind surface shear. The effect of the wind stress is more pronounced in shallow coastal. In addition to the daily variability associated with the sea and land breeze, the prevailing wind is northerly during the summer and of southerly during the winter.

Figure 16 indicates two points, in which the wind velocity was calculated using the data from the MM5 with a resolution of 9km.

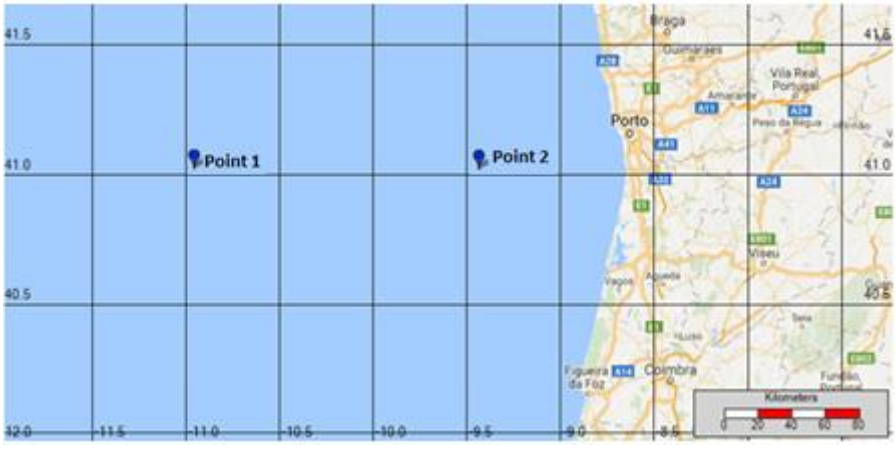

Figure 16 - Location of the points to calculate the wind velocity

Observing the wind roses it is possible to conclude that the prevailing wind is northerly during the summer, between June and August of 2011. During this period, 20 to 30 % of the wind speed varies between 40 to 50 km/h (Figure 17).

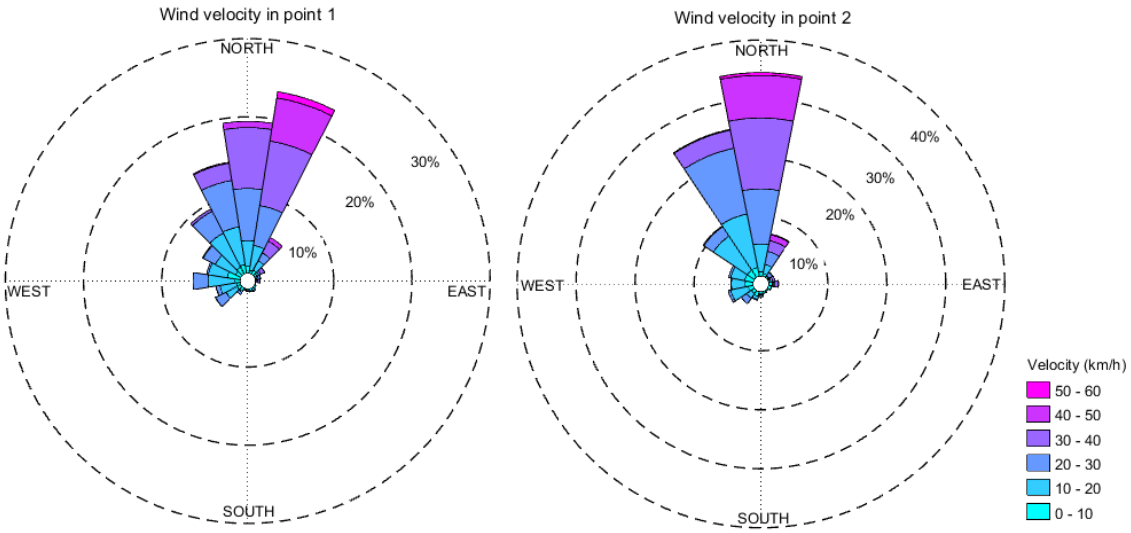

Figure 17 - Wind roses for the points referred in Figure 16.

For a northerly wind, characteristic of the spring/summer months, Figure 18, the density gradient is not sufficient to maintain a northward current and the latter eventually switches south. Analysing the wind diagram, it is possible to verify at 41ºN, during the same period, occurred intense northerly winds (30-40 km/h).

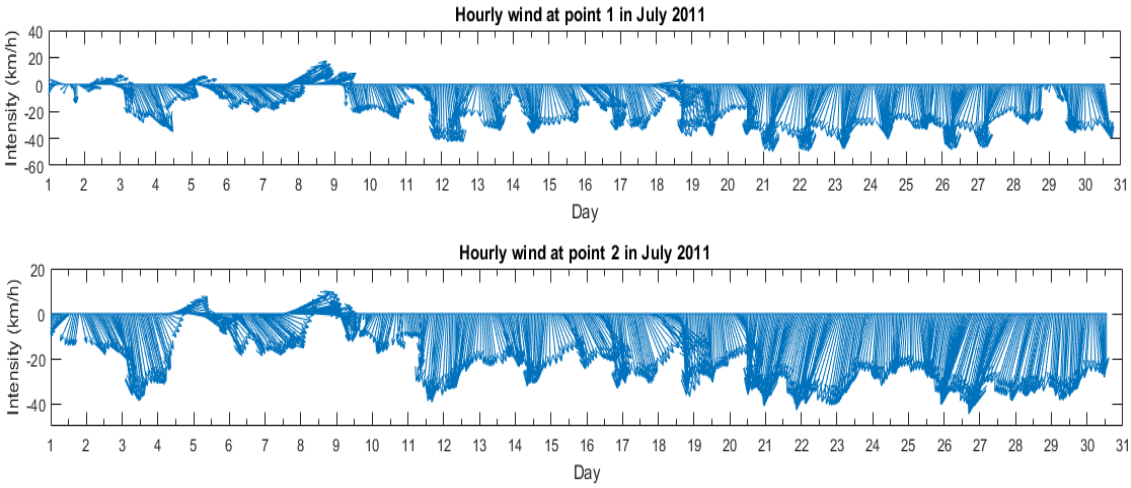

Figure 18 - Stick diagram showing directions and velocities (km/h) of the wind for point 1 and 2 (negative values correspond to northerly winds).

Due to the Ekman transport, the prevailing winds along the Portuguese coast give origin to two types of mixed layer circulation: during the upwelling period, with northerly winds, surface waters are transported offshore which results in a divergence along the coast and lowering of the sea-level. During the period in which southerly winds dominate, Ekman's transport occurs towards the coast, there is coastal convergence and the sea-level rises along the coast.

The Ekman velocities (U_e) were calculated for the same period of the upwelling event (Figure 19) based on the wind data at 12 a.m. provided by MM5 according to the equation:

$$U_e = \frac{\tau_y}{\rho f d} \quad (10)$$

Where ρ is the water density (1026.0 kg/m^3), f is the Coriolis parameter (~1x10^4 s^{-1} for 41ºN), and d is the depth of the Ekman layer (10 m), the same values used by Ribeiro et al. (2005).

The meridional component of the wind stress (τ_y) was calculated according to:

$$\tau_y = \rho_a C_d V_y |V| \quad (11)$$

Where ρ_a is the density of the air (1.2 kg/m^3), C_d is the drag coefficient (0.0015), V_y is the wind velocity along the y direction and $|V|$ is the wind velocity modulus, the same values used by Ribeiro et al. (2005).

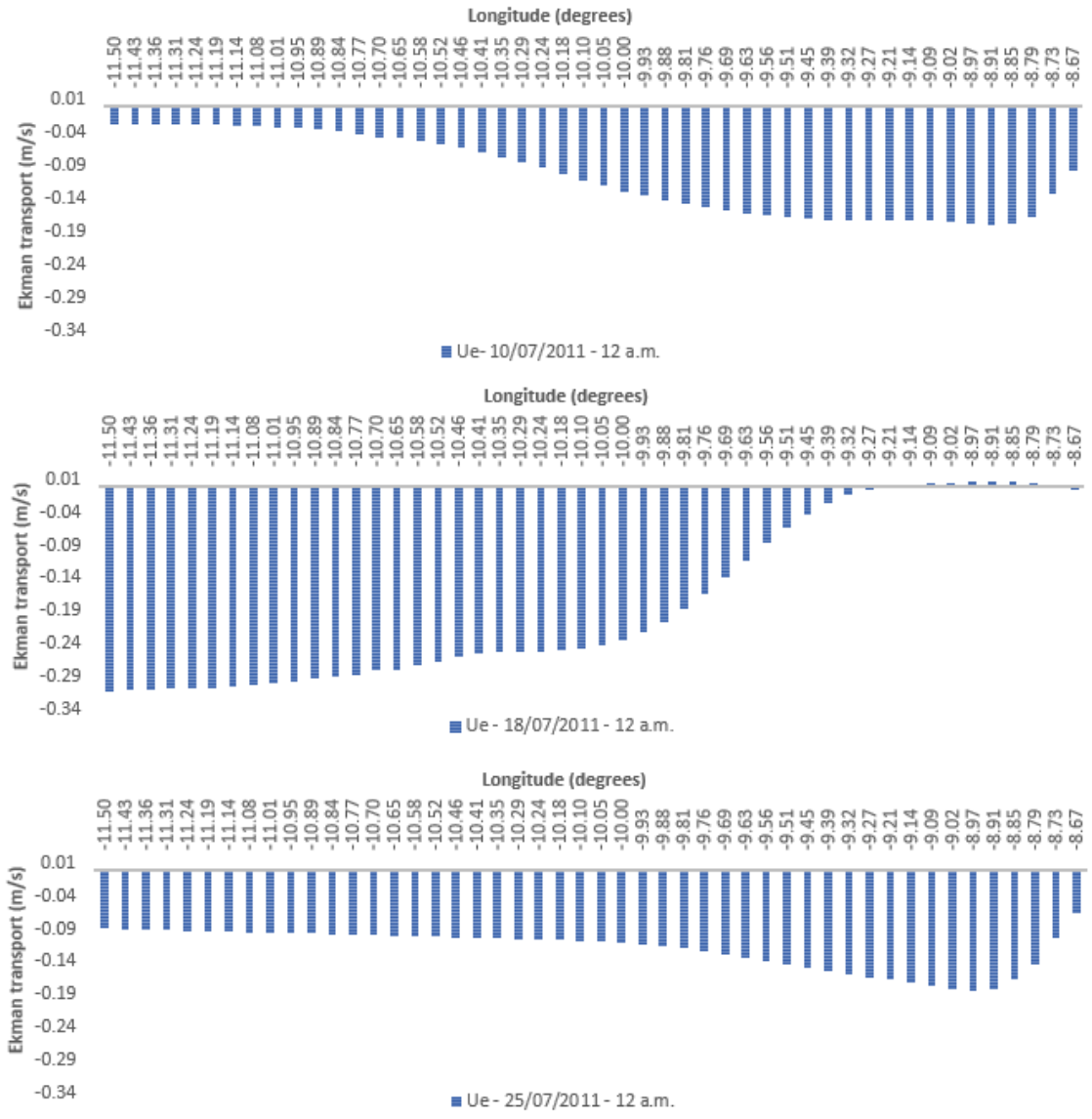

Figure 19 - Diagram showing Ekman velocities (m/s) for each longitude (between -8.67º and -11.5º).

4. Validation of the hydrodynamic model

4.1. Model errors statistics

Model errors derive from inaccuracies in process descriptions, parameterization constants, initialization, forcing functions, and boundary conditions.

The percentage model bias (the sum of model error normalized by the data) indicates whether the model is overestimating or underestimating the observations, the results of the model being better the smaller the bias.

Some performance levels are categorized as follows: |bias| <10 excellent, 10–20 very good, 20–40 good, >40 poor (Babovic et al., 2005)

The bias is given by:

$$Bias = \frac{\sum_{n=1}^{n} |M_n - D_n|}{\sum_{n=1}^{n} Dn} \quad (12)$$

Where M is the model estimation, D the data and t the time index, respectively

The root mean squared error (RMS) of n model-data comparisons (total grid points) is defined by the next equation. The closer the RMS is to zero the better is the fit between the model and observations. Thus, the RMS can be obtained by:

$$RMS\ error = \frac{1}{n} \sqrt{\sum_{n=1}^{n} (M_n - D_n)^2} \quad (13)$$

The correlation coefficient (R) express the quality of a least squares fitting between the model and data (R= 0 no relationship, R= 1 perfect fit). The square of the correlation coefficient (R^2) expresses the percentage of the variability in data that can be accounted for by the model.

The R coefficient is calculated using:

$$R = \frac{\sum_{n=1}^{n} (Dn - \overline{Dn})\ (Mn - \overline{Mn})}{\sqrt{\sum_{n=1}^{n} (Dn - \overline{Dn})^2\ \sum_{n=1}^{n} (Mn - \overline{Mn})}} \quad (14)$$

Figure 20 shows the statistical analysis of the MOHID model for SST values. The analysis is made in three days (10 July 2011, 18 July 2011 and 25 July 2011) using satellite data from ODYSSEA for SST, which provide daily gap-free maps of SST, at 0.02º x 0.02º horizontal resolution, using infra-red and micro-wave radiometers covering the Portugal domain.

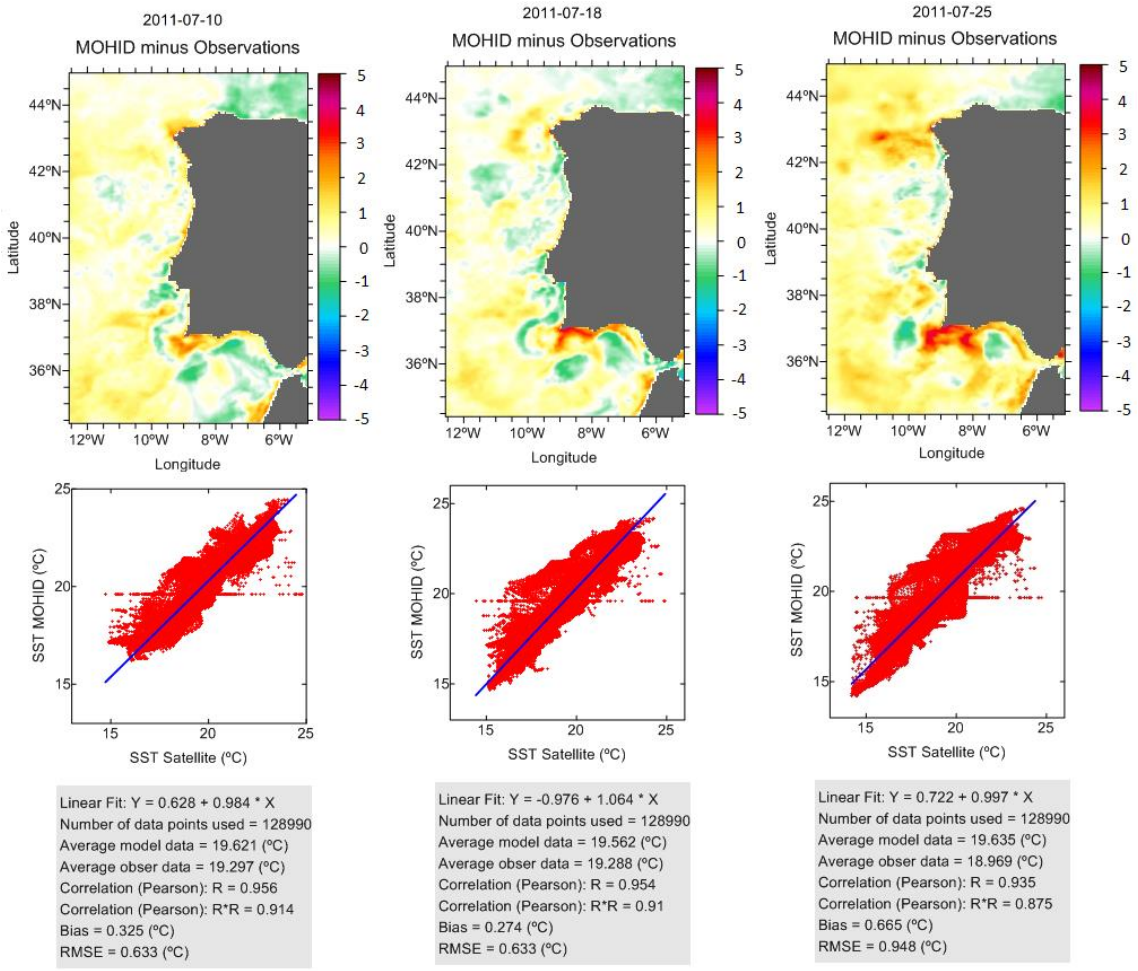

Figure 20 - Statistical parameters between the SST from satellite and SST from MOHID.

In the three days, the MOHID model has a correlation higher than 0.93. On the 10th of July R = 0.956 and RMSE = 0.633ºC and the bias coefficient equals 0.325ºC, which means that the model overestimates SST observations. On the 18th of July R = 0.954 and RMSE kept unchanged. The bias coefficient is also the same, which means that the model continues to overestimate the SST observations. On the 25th of July, the correlation coefficient is slightly lower than the previous ones (R = 0.935) and the RMSE has the highest value (0.948ºC). In general, the comparison shows that the difference between the MOHID results and satellite observations is very small, not exceeding 1ºC.

4.2. Argo buoy

Argo buoys are a global array of 3800 free-drifting profiling floats that measure the temperature and salinity in the upper 2000 m of the ocean. They enable, for the first time, continuous monitoring of the temperature, salinity, and velocity of the upper ocean, with all data being relayed and made publicly available within hours after collection.

These floats sink to a target depth of 1000m, then drift and sinks again to 2000m, before they start measuring the temperature and salinity profile. The data come from battery-powered autonomous floats that spend most of their life drifting at a depth where they are neutrally buoyant (the "parking depth"). Periodically, approximately each ten day, the Argo buoy rises to the surface, measuring vertical profiles of conductivity, temperature and pressure from which it is possible to calculate the salinity and the density of the water. The observations are transmitted via satellite to information gathering centers, located on land, allowing scientific studies of the oceans. This cycle is illustrated in Figure 21.

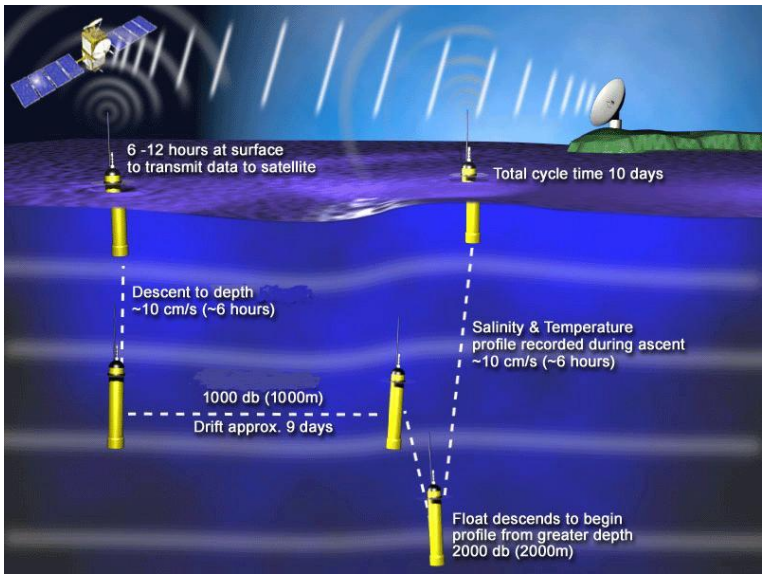

Figure 21 - Argo buoy scheme (source: http://www.argo.ucsd.edu/How_Argo_floats.html).

The observations of the Argo buoys found on the Portuguese coast were used for the validation of the model. Throughout this section, a comparison is made between the temperature and salinity along the water column, of Argo buoys observations and the results of Mercator and MOHID models (Figure 22 and Figure 23). In the following figures in the upper left corner is represented the temperature, in the upper right corner the salinity, in the lower left corner the T-S diagram and in the lower right corner the location of the Argo buoy in the model domain. Figure 23 presents the on June 14, 2011 and Figure 23, on June 24, 2011.

On June 14 (Figure 22), it is possible to verify that the results of the MOHID baroclinic model agree quite well with the observations and the results of the Mercator model. On the whole, the agreement of the MOHID results with the temperature observations is slightly lower than the Mercator model, since the correlation coefficient is equal to 0.991 for the former and 0.994 for the latter.

The RMSE value is also slightly lower in the Mercator observations (0.284ºC) than in the MOHID model (0.346ºC). Regarding the bias, both the Mercator and the MOHID models have an excellent performance. In relation to salinity, the results from Mercator are also slightly better, with a correlation coefficient of 0.958 against a correlation coefficient of 0.952 for the MOHID model. However, both models have a good agreement with the data from Argo. For instance, the RMSE for Mercator is 0.044 and for the MOHID model is 0.054.

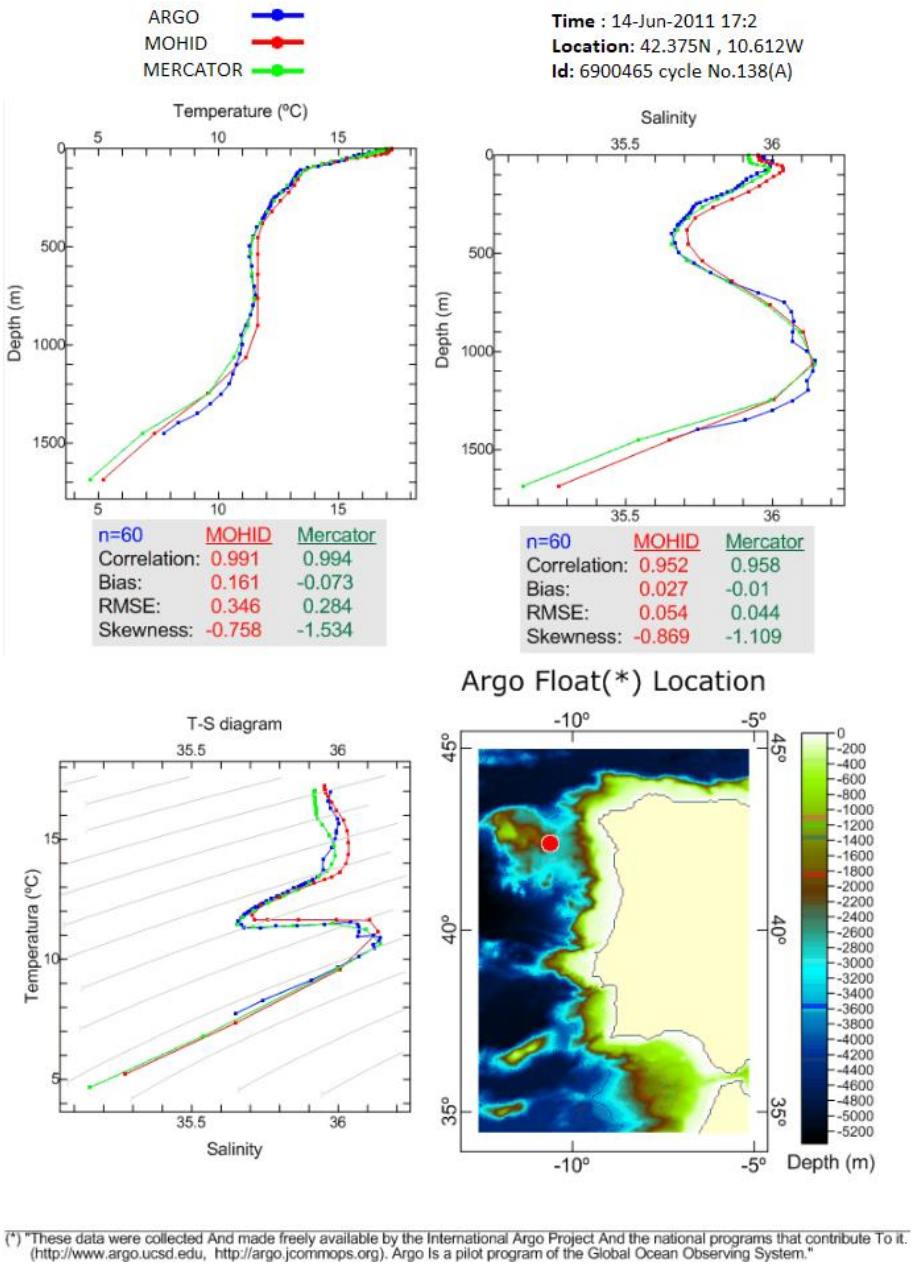

Figure 22 - Comparison between the data from MOHID model and the Argo buoys on 14 June 2011.

In the Figure 23, it is possible to verify that the results of the MOHID baroclinic model once again, agree well with the observations and with the results of the Mercator model. Regarding temperature, both models have excellent performances with the same correlation coefficient R= 0.998. The RMSE value is slightly higher in the MOHID model (0.241ºC) than in the Mercator (0.231ºC). Considering the bias, both models have an excellent fit against the Argo data. In relation so salinity, the results are less accurate, especially in the upper 100m, i.e., the mixed layer and around 1000m depth, the level of Mediterranean water. Despite the discrepancies between the Mercator model and the observations, the MOHID model manages to mitigate these errors and, on the whole presents better results, as can be seen from the statistical parameters.

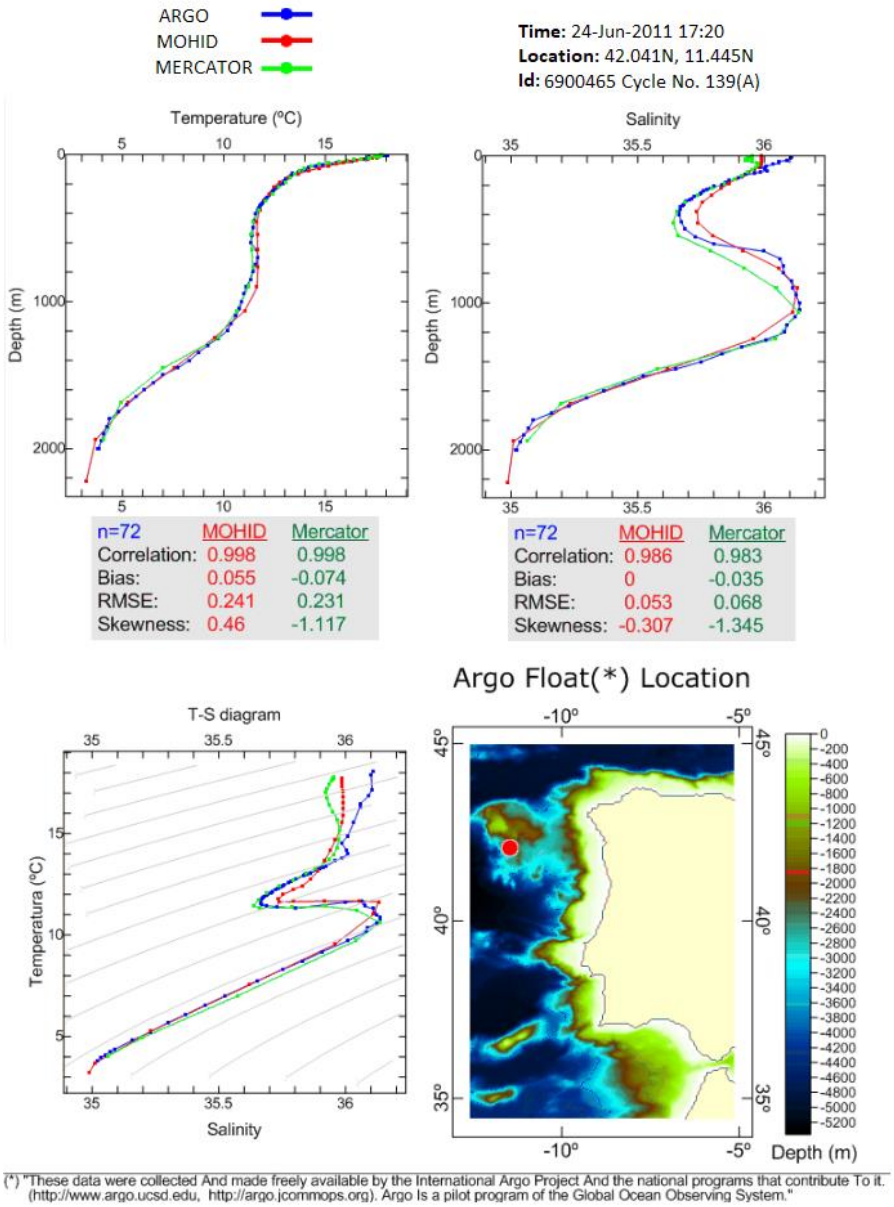

Figure 23 - Comparison between the data from MOHID model and the Argo buoys on 24 June 2011.

5. Results and Discussion

In this section the results of the two scenarios are presented and analysed. The area under observation is located between 40ºN and 42ºN and approximately 3º offshore (11ºW) from the coast. SST values obtained from the model and satellite observations are compared, in order to validate the results of MOHID. In addition, alongshore velocities in a cross-section located at 41ºN will be analysed.

5.1. SST comparison between the model results with WIBP and satellite images

The comparison of model results and satellite images are shown in Figure 24 for the period between 10 July 2011 and 25 July 2011. This period corresponds to the beginning of the upwelling event until the filament, located around 41ºN, reaches its maximum extension.

In the satellite imagery of 10 July (Figure 24a), 18 July (Figure 24b) and 25 July (Figure 24c), it is possible to observe the beginning of an upwelling event, as well as the development of a filament near 41ºN. The filament is associated with a strong offshore surface current, consistent with its westward propagation, reaching approximately 150 km in length (~2º), on July 25 (Figure 24c). The lighter waters at the surface layer of the filament, are colder (~14 – 15ºC) than the surrounding waters (~16-17ºC), providing a buoyancy force that boosts its propagation.

Comparing the results of MOHID with satellite images, it is possible to conclude that it is a reliable numerical tool, being able to reproduce the development of the Aveiro filament (red rectangles in Figure 24c, Figure 24g and 25). The zooms in the region of the filament for the satellite images (Figure 24d) and model results (Figure 24h), show a good agreement in SST, as well as in the shape and extension of the filament, which reaches approximately 150 km after fifteen days of upwelling.

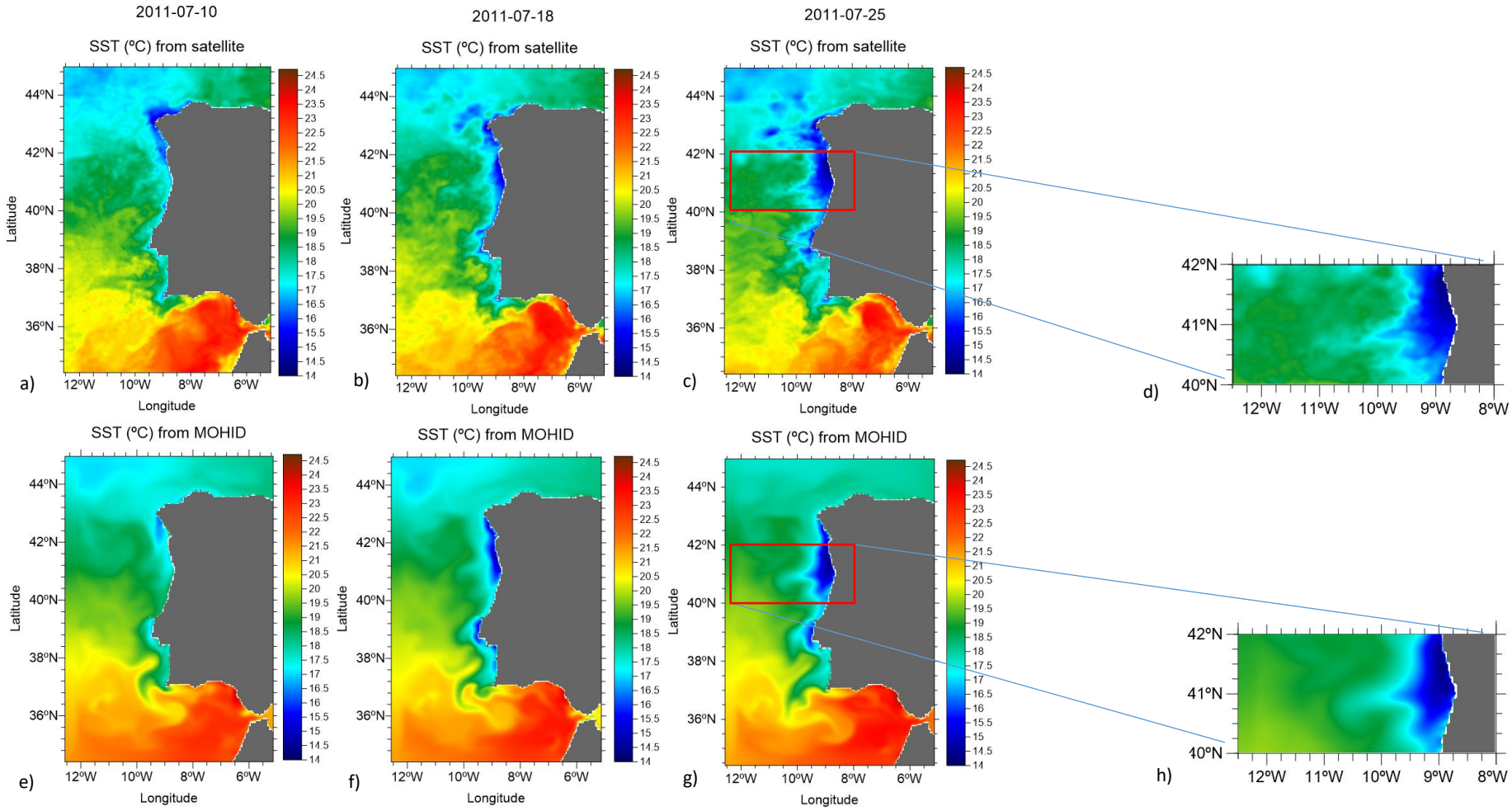

Figure 24 – SST from satellite on (a) 10 July, (b) 18 July and (c) 25 July 2011 and results from MOHID model, on (e) 10 July, (f) 18 July and (g) 25 July. On (d) and (h) is represented a zoom in the study area.

5.2. The WIBP impact

5.2.1. Comparison of SST with numerical results

In order to verify the impact of the salinity signature of the WIBP on the formation of the Aveiro filament, a second scenario was implemented. The coastal fresher water was removed and replaced by saltwater with a salinity equal to 35.9 psu. Looking at Figure 25, which represents the filament at its maximum extension, it is evident that the change introduced in the initial conditions of salinity has a negligible impact on the extension of the filament, but a relevant one in its orientation, since there is a southward shift. This displacement can be explained by a stronger upwelling jet, as can be observed in the vertical cross-sections presented in Figure 27.

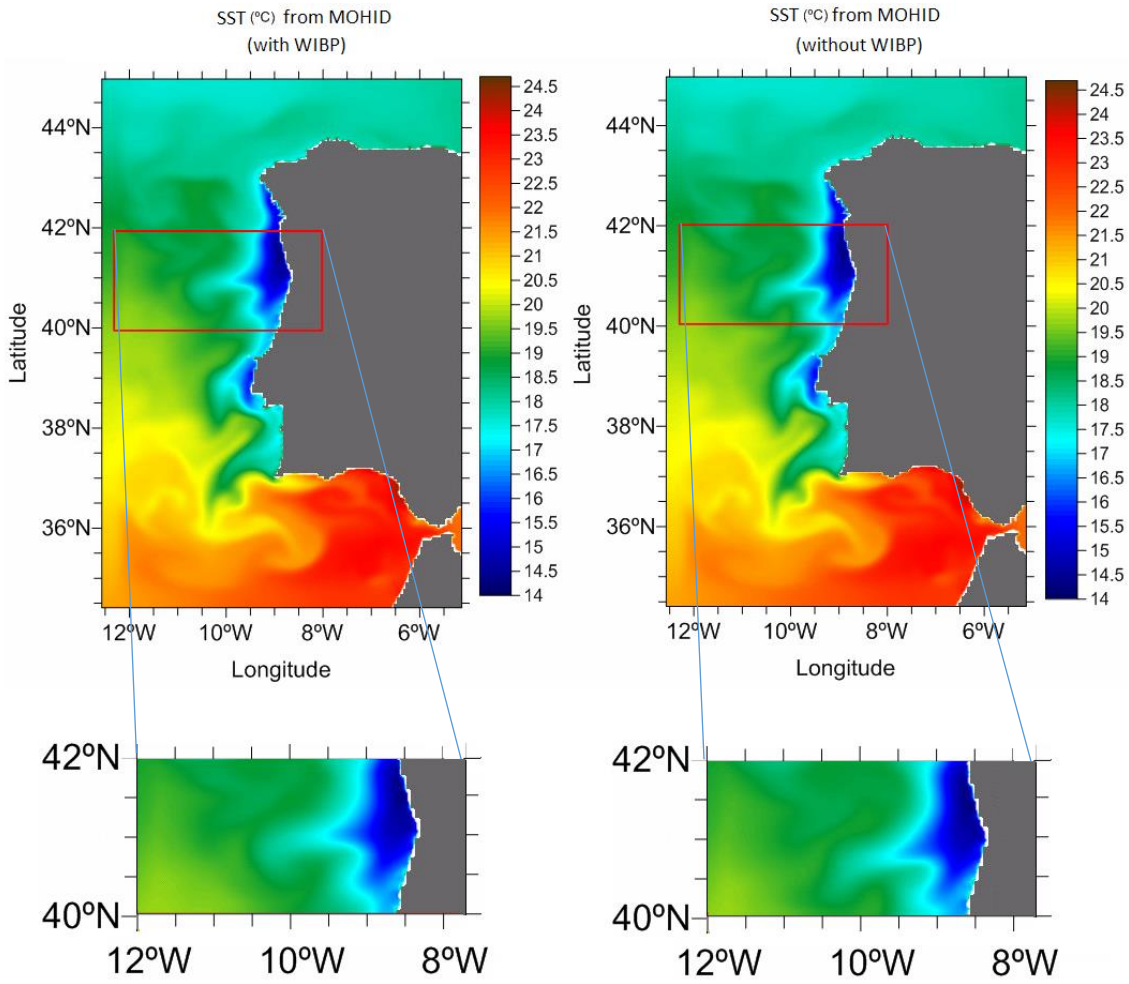

Figure 25 – SST values for MOHID, with WIBP (left) and without WIBP (right) on 25 July 2011.

5.2.2. Vertical cross-sections

In order to have a better understanding of the WIBP impact, vertical cross-sections of the flow (Figure 27) at 41ºN were also analysed, for the same period of the SST images. Figure 26 shows the SST and horizontal velocity fields obtained with the MOHID model for 25 July at 12 a.m., clearly representing a typical upwelling circulation.

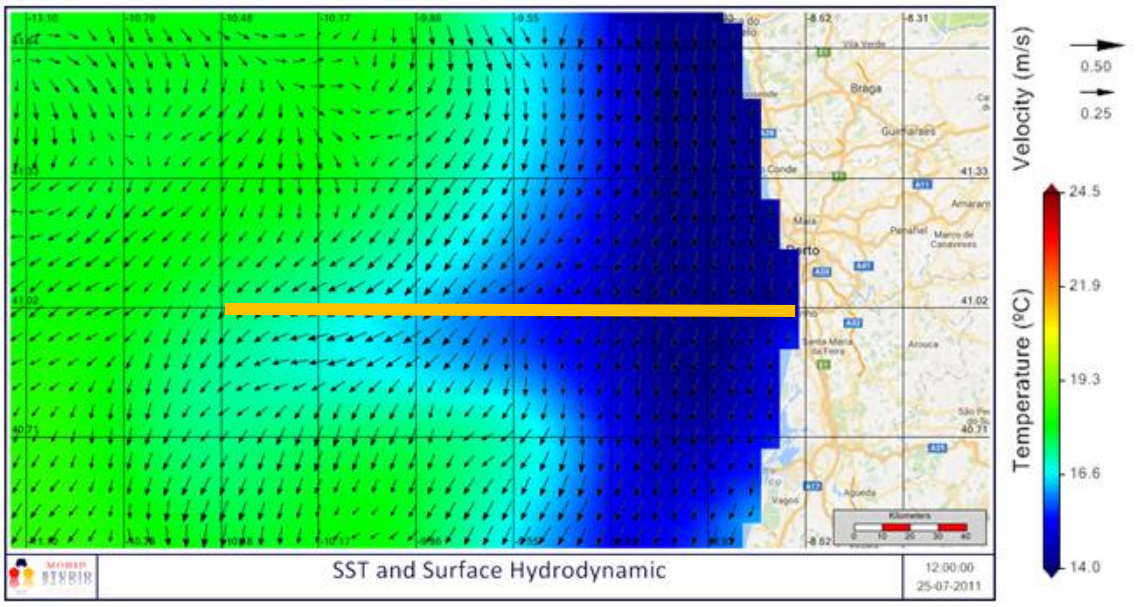

Figure 26 –SST (colours) and surface velocity fields (arrows) obtained with the MOHID model with WIBP for 25 July at 12 a.m. The yellow line represents the location of the vertical cross-section where the flow was subsequently analysed.

Figure 27 shows the alongshore velocity and density anomalies, for the section mentioned above, considering both scenarios, i.e., with and without the salinity effect of the WIBP. Typical patterns of a summer upwelling event in the western Portuguese coast are present, namely, along-shore velocities mostly negative (southward) and surface-intensified, as well as a costal counter-flow.

Southward alongshore velocities range from -0.1 (Figure 27a) to -0.25 m/s at the surface (Figure 27b). In Figure 27c) it is possible to identify the double upwelling front, approximately between -9.5º and -9.7º , as mentioned by Peliz et al. (2002) in their conceptual scheme (Figure 4 in this work). Although slightly less intense than in their observations, the upwelling jet is still clearly visible.

Offshore of the upwelling jet, a poleward flow is observed in Figure 27a and Figure 27c, located between -11º and -10.3º, with velocities around 0.03 m/s. This poleward flow has been documented along all eastern boundaries and, in our study region, it corresponds to the IPC, mentioned by Peliz et al. (2005) and Torres et al. (2007). Although its location changes seasonally, during a summer upwelling event it may interact with the filament, acting like a barrier that hinders its offshore advection.

Otero et al. (2008), concluded that the offshore spreading of the WIBP is highly influenced by the wind regime and the mesoscale circulation (i.e. the PCC and IPC). They also concluded that the WIBP is confined at the coast when poleward winds prevail, being exported offshore and southward under upwelling favourable winds. Another study by Rossi et al. (2013) shows that the freshwater from the WIBP may be advected inside the filament as far as 140 km offshore.

In addition to the previous remarks regarding the contribution of the mesoscale circulation and the WIBP to the propagation of the filament, Peliz et al. (2002) suggest that an anticyclonic eddy may be formed between the IPC and the upwelling jet, improving the offshore extension of the filament. No signs of such eddy were observed in MOHID results.

The previous comments concern the simulation with the WIBP. In what regards the impact of the WIBP, comparing Figures 27c and 27f the main conclusion is that the buoyant plume affects primarily the intensity and vertical extension of the upwelling jet, more conspicuous in the case without the salinity signature of the WIBP. A possible explanation for this is based on the fact that, without the WIBP, coastal waters become denser and, therefore, the upward slope of the isopycnals towards the shore creates a baroclinic pressure force that reinforces the southward flow. Actually, looking at Figure 27i, the green area, roughly at the same position of the core of the upwelling jet, corresponds to denser water without WIBP.

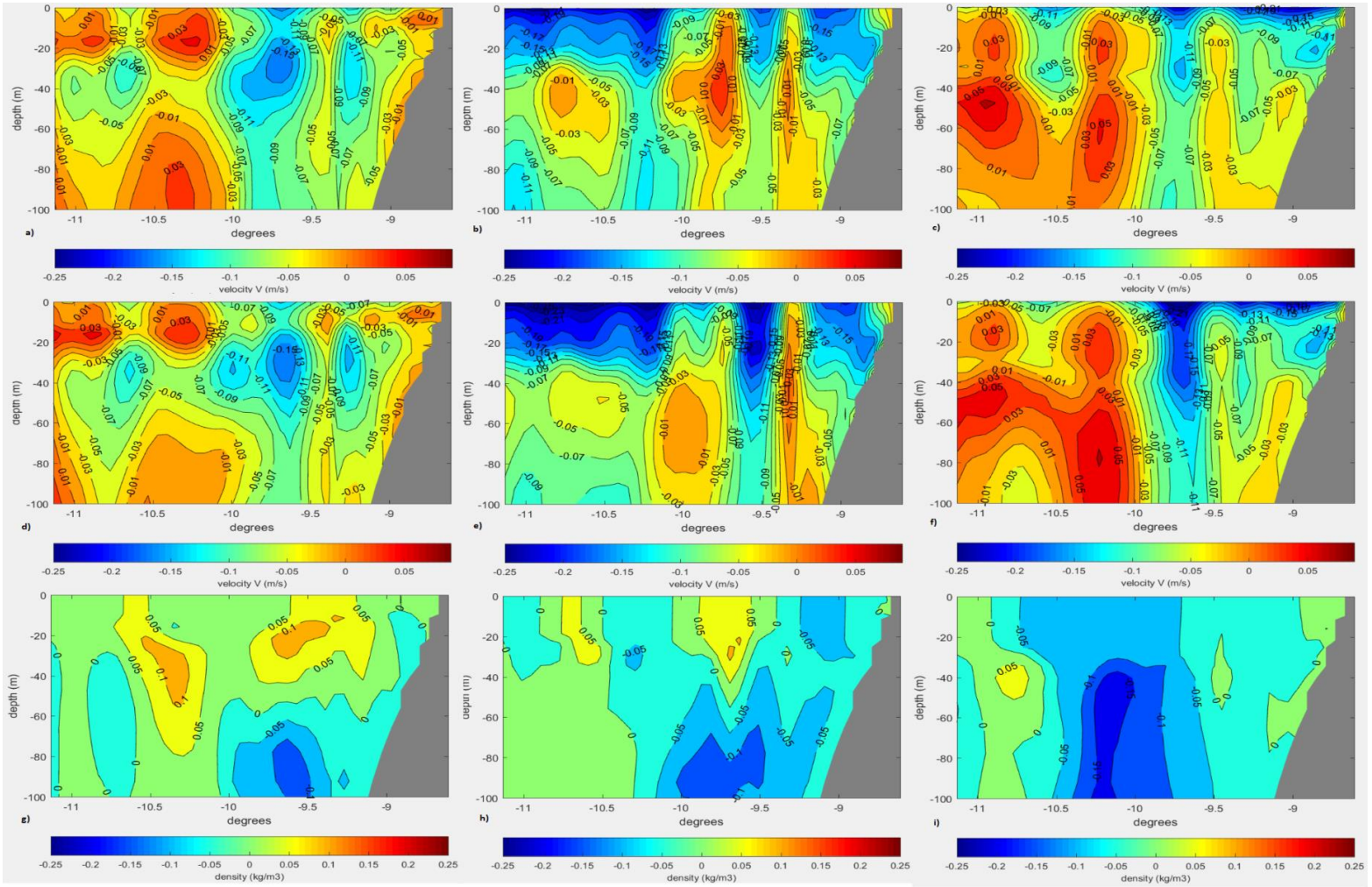

Figure 27 - Vertical cut at 41ºN during the upwelling event. Images a), b), and c) presents the North (positive values) and South (negative values) velocities (with WIBP) for 10 of July, 18 of July and 25 of July 2011, respectively; Images d), e), and f) presents the along-shore velocities (without WIBP) for the same days; Images g), h), and i) presents the differences between density anomalies without and with WIBP.

5.2.3. MOHID differences between the two scenarios

Figure 25 shows the difference in SST between the simulations with and without the salinity signature of the WIBP. The red and blue spots at the latitude of the Aveiro filament may be explained by its southward displacement. Superimposed to this effect, there may also be differences in the thermal gradient across the filament for the two scenarios. This subject needs further research. Another interesting observation is that changing the salinity of the WIBP also affects the filaments formation in the Cape Roca.

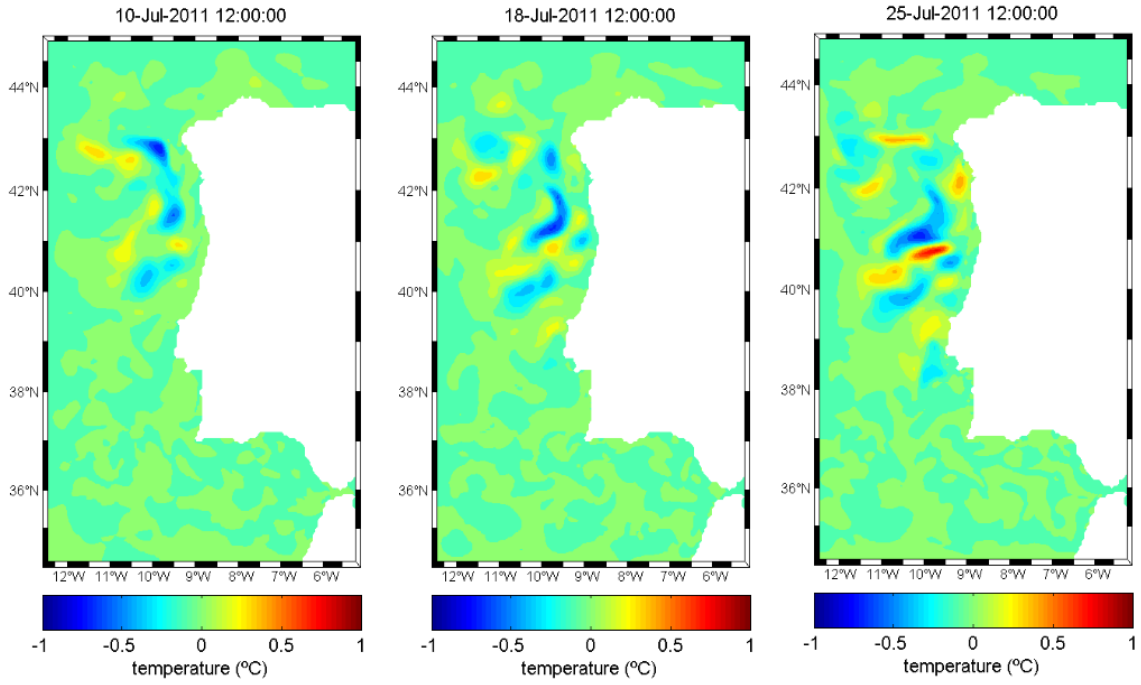

Figure 28 - Differences between SST obtained for the simulations with WIBP and without WIBP, for 10 July, 18 July and 25 July, respectively.

5.3. Comparison between MOHID model and Lentz's model

.

It is interesting to compare the filament extension obtained with the MOHID model, with the results of an analytical model. The model chosen was the Lentz's model (2004). Since it is two-dimensional, there are no changes along the alongshore distance, i.e., $\partial/\partial y = 0$. The initial configuration (subscript i) is shown in Figure 29, the buoyant coastal plume occupying the region above the broken line.

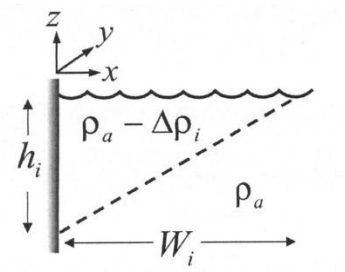

Figure 29 - Initial configuration (broken line) of the buoyant coastal plume (Source: Lentz, 2004).

Immediately after the onset of wind forcing (subscript o), Lentz considers two possible cases: if the wind is sufficiently strong, entrainment occurs in the whole plume (Figure 30 on the right), otherwise only part of the plume is affected (Figure 30 on the left).

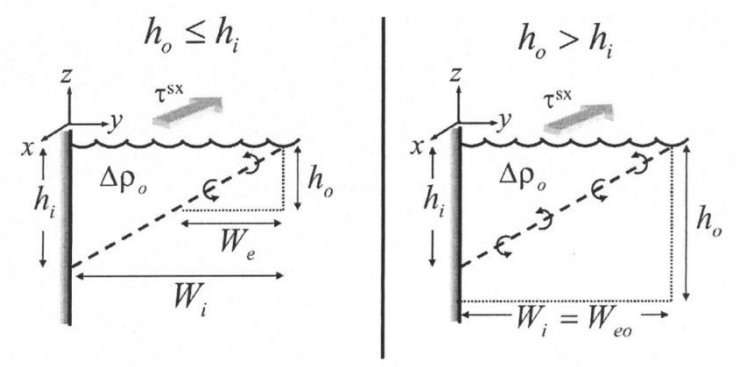

Figure 30 - Immediately after the onset of wind forcing, there are two possible cases: on the left, the entrainment does not affect the whole plume, contrary to what happens on the right (Source: Lentz, 2004).

Due to the wind, a surface mixed layer forms at the offshore edge of the plume. The wind tends to deepen it, while buoyancy has a stabilizing effect. When the two effects balance each other, the system can be described by a constant value of a critical Richardson number given by $Ri_c = \frac{g\Delta\rho_o h_o}{\rho_a|\Delta u|^2} \approx 1$, where $\Delta\rho_o$ is the density anomaly of the plume after the onset of wind forcing, h_o is its thickness at the offshore edge and $|\Delta u| = U_E/h_o$ the velocity jump at the base calculated with the Ekman transport $U_E = \tau^{sy}/\rho_a f$.

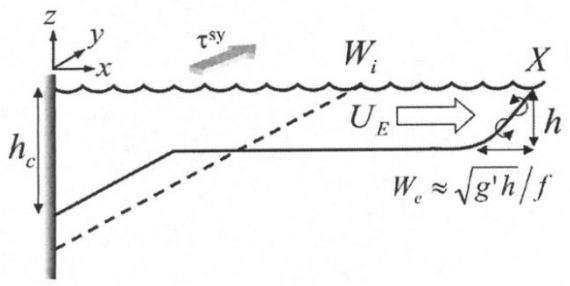

Figure 31 - Wind-driven entrainment at the offshore edge of the plume. The dashed line represents the initial shape of the plume (Source: Lentz, 2004).

Schematically, the entrainment at the offshore edge of the plume is considered to be a two-step process: firstly, there is a geostrophic adjustment in a distance equal to the internal Rossby deformation radius (W_e in Figure 31), followed by wind-driven mixing. Actually, the two processes occur simultaneously in an entrainment area roughly equal to $A_e = W_e h/2$. To calculate the position of the offshore edge of the plume $X(t)$, Lentz uses six equations, which are presented next in sequential order of calculus:

$$h_s = \left(\frac{2Ri_c\rho_a U_E^2}{g h_i \Delta\rho_i}\right)^{1/2} \quad \text{with} \quad U_E = \tau^{sy}/\rho_a f \tag{15}$$

$$\begin{cases} \tilde{h}_o^3 - \tilde{h}_s^2\left(\tilde{h}_o^2 + 1\right)/2 = 0, & \tilde{h}_s \le 1 \\ \tilde{h}_o = \tilde{h}_s, & \tilde{h}_s > 1 \end{cases} \quad \text{with} \quad \tilde{h}_s = h_s/h_i \tag{16}$$

$$\Delta\rho_o = \begin{cases} \Delta\rho_i\left(1 + \tilde{h}_o^2\right)^{-1}, & \tilde{h}_o \le 1 \\ \Delta\rho_i\left(2\tilde{h}_o\right)^{-1}, & \tilde{h}_o > 1 \end{cases} \tag{17}$$

$$h_o = \left(\frac{Ri_c\rho_a U_E^2}{g\Delta\rho_o}\right)^{1/3} \tag{18}$$

$$A_o = \begin{cases} A_i\left(1 + \tilde{h}_o^2\right), & \tilde{h}_o \le 1 \\ 2A_i\tilde{h}_o, & \tilde{h}_o > 1 \end{cases} \tag{19}$$

$$X = W_i + \frac{3A_o}{\sqrt{Ri_c}h_o}\left[(1+\hat{t})^{2/3} - 1\right] \quad \text{with} \quad \hat{t} = t/t_s = t/\left(\frac{2A_o}{\sqrt{Ri_c}U_E}\right) \tag{20}$$

where t_s is the time it takes to double the cross-sectional area from A_o to $2A_o$, the initial cross-sectional area being $A_i = W_i h_i/2$. Variable $\tilde{h}_o = h_o/h_i$ represents the normalized thickness at the offshore edge of the plume, immediately after the onset of wind forcing. Densities can be calculated using the equation of state (Cushman-Roisin, 2008):

$$\rho = \rho_0[1 - \alpha(T - T_0) + \beta(S - S_0)] \tag{21}$$

where the constants ρ_0, T_0, S_0 are reference values of density, temperature and salinity, respectively, α is the coefficient of thermal expansion and β the coefficient of saline contraction. Typical seawater values are $\rho_0 = 1028\, kgm^{-3}$, $T_0 = 10\, ºC$, $S_0 = 35\, psu$, $\alpha = 1.7{\times}10^{-4} K^{-1}$, $\beta = 7.6{\times}10^{-4}$.

The input parameters used are:

$T_a = 17\, ºC, T_i = 19\, ºC, S_a = 36\, psu, S_i = 35.5\, psu, \tau^{sy} = 0.09\, Pa, h_i = 30\, m, W_i = 5\, km.$

For these values $\boldsymbol{X \approx 156\ km}$ after 15 days of upwelling, which is similar to the value obtained numerically ($\approx 150\, km$) for the offshore extension of Aveiro filament. If we consider $S_i = S_a$, keeping constant the other values, the effect of fresher water is discarded and $\boldsymbol{X \approx 122\ km}$, i.e., a reduction of 22 % in the offshore distance reached by the plume. Likewise for the temperature. If we consider $T_i = T_a$, keeping constant the other values, the effect of the temperature signature of the WIBP is no longer considered and $\boldsymbol{X \approx 127\ km}$, which represents a reduction of 19 %. These changes were not observed with the MOHID model, which means that further research is needed. It is interesting to compare the impact of the temperature and salinity signatures. From equation (21), one obtains $dS = -(\alpha/\beta)dT = -0.224dT$, for the same change in density. In other words, a decrease of 2 ºC (the difference between T_i and T_a) has an effect on density equivalent to an increase in salinity of 0.448 psu. For the present case, this means that the impact of the salinity and temperature signatures are almost equivalent, with a slightly higher contribution of the former, as confirmed by the results of the Lentz's model.

It is important to keep in mind that Lentz's model does not simulate the generation of upwelling filaments. The existence of these hydrodynamic features requires alongshore variations of offshore propagation of coastal waters, a restriction excluded from Lentz's model since it is two-dimensional. In addition, filaments are prone to baroclinic instabilities (which explains why eddies are ubiquitous whenever filaments are present) and such instabilities are not considered in Lentz's model. However, the Aveiro upwelling filament is closely related to the offshore transport of a buoyant plume, which was the main reason for having chosen Lentz's model, despite its inaccurate description of the local hydrodynamics. In this regard, we should be aware of the fact that the offshore propagation of the Aveiro filament is counteracted by currents with a relevant meridional component, such as: the southward upwelling jets and, further offshore, the IPC and the PC. On the other hand, according to Peliz et al. (2002), the offshore propagation can be boosted by an anticyclonic eddy formed between the upwelling jet and the IPC. Neither the aforementioned currents nor the anticyclonic eddy are taken into account in Lentz's model.

6. Conclusions and Future work

In the course of this work the main issues that had to be solved, in order to have a proper implementation of the MOHID model, were related to instabilities originated in the bathymetry and the downscaling process. In particular, the difficulty in imposing adequate boundary conditions for downscaling, led us to abandon this methodology and the simulations were performed only with the PCOMS model bathymetry.

In spite of these difficulties, the MOHID model allowed us to reach firm and systematic conclusions, revealing its capacity to simulate coastal hydrodynamic processes, namely, coastal upwelling.

To study the interaction between the buoyant coastal plume and upwelling filaments is a hard task to fulfil, for a variety of reasons that include variable winds and environmental conditions, interaction of phenomena with different geophysical scales, complex bathymetry, etc..

Despite all the difficulties, the main conclusion of this work was that the salinity signature of the WIBP does not change the extension of the Aveiro filament. However, it has a relevant impact in the filament orientation. Changing the salinity in the WIBP, intensifies the upwelling jet, which is responsible for the southward displacement of the filament. In addition, it also affects the Cape Roca filaments formation.

As a future work, to gain a deeper insight into WIBP's contribution to Aveiro filament formation, it might be interesting to apply a different methodology comparing two simulations with and without the river discharges. The short time available for this work and the computational limitations have prevented this approach.

The ecological implications were out of the scope of the present study, but it would also be interesting to assess the effect of the WIBP on the primary production (phytoplankton, etc.) inside the filament.

References

Babovic, Vladan, S. A. Sannasiraj, and Eng Soon Chan. 2005. “Error Correction of a Predictive Ocean Wave Model Using Local Model Approximation.” *Journal of Marine Systems* 53(1–4):1–17.

Bakun, Andrew, David B. Field, Ana Redondo-Rodriguez, and Scarla J. Weeks. 2010. “Greenhouse Gas, Upwelling-Favorable Winds, and the Future of Coastal Ocean Upwelling Ecosystems.” *Global Change Biology* 16(4):1213–28.

Borges, M. F., A. M. P. Santos, N. Crato, H. Mendes, and B. Mota. 2003. “Sardine Regime Shifts off Portugal: A Time Series Analysis of Catches and Wind Conditions.” *Scientia Marina* 67(S1):235–44. Retrieved (http://scientiamarina.revistas.csic.es/index.php/scientiamarina/article/view/523/536).

Braunschweig, F.; Leitao, P. C.; Fernandes, L.; Pina, P; Neves. 2002. “The Object Oriented Design of the Integrated Water Modelling System.” 1–12.

Burchard, H. .. K.Bolding and M. R.Villarreal. 1999. “GOTM, A General Ocean Turbulence Model.” *Rep. of EC, EUR 18745 EN* Theory, im.

Castro, Carmen G., F. F. Pérez, X. A. Álvarez-Salgado, and F. Fraga. 2000. “Coupling between the Thermohaline, Chemical and Biological Fields during Two Contrasting Upwelling Events off the NW Iberian Peninsula.” *Continental Shelf Research* 20(2):189–210.

Coelho, H. S.; Neves, R. R.; Leitão, P. C.; Martins, H.; Santos, A. P. 1998. “The Slope Current along the Western European Margin: A Numerical Investigation.” *Boletin Instituto Espanol de Oceanografia* 61–72.

Coelho, H. S., R. R. Neves, P. C. Leitão, H. Martins, and a P. Santos. 1999. “The Slope Current along the Western European Margin : A Numerical Investigation.” *Bol. Inst. Esp. Oceanogr.* 15(1–4):61–72.

Cravo, Alexandra et al. 2010. “An Upwelling Filament off Southwest Iberia : Effect on the Chlorophyll a and Nutrient Export.” 30(October 2004):1601–13.

Cushman-Roisin, B. a. 2008. *Introduction to Geophysical Fluid Dynamics, Physical and Numerical Aspects*. edited by Academic Press.

Decyk, V. K.; Norton, C. D.; Szymanski, B. K. 1997. “Expressing Object-Oriented Concepts in Fortran90.” *ACM Fortran Forum*.

Drinkwater, Kenneth F. et al. 2003. “The Response of Marine Ecosystems to Climate Variability Associated with the North Atlantic Oscillation.” *The North Atlantic Oscillation: Climatic Significance and Environmental Impact. Geophyiscal Monograph 134.* 211–34.

Fernandes, R. 2005. “Modelação Operacional No Estuário Do Tejo.” Instituto Superior Técnico,

Universidade Técnica de Lisboa.

Fiúza, A. F. D., M. E. de Macedo, and M. R. Guerreiro. 1982. “Climatological Space and Time Variation of the Portuguese Coastal Upwelling.” *Oceanologica Acta* 5(1):31–40. Retrieved (http://archimer.ifremer.fr/doc/00120/23169/21014.pdf).

Fraga, F. 1992. “Water Masses in the Upper and Middle North Atlantic Ocean East of the Azores.” (3).

Frouin, Robert, Armando F. G. Fiúza, Isabel Ambar, and Timothy J. Boyd. 1990. “Observations of a Poleward Surface Current off the Coasts of Portugal and Spain during Winter.” *Journal of Geophysical Research* 95(C1):679.

Garrido, Susana, Maria Emilia Cunha, Paulo B. Oliveira, and Carl D. Van der Lingen. 2006. “Diet Composition and Feeding Behaviour of Iberian Sardine (Sardina Pilchardus).” *ICES Journal of Marine Science* 17:21.

Gomes, N. 2014. “Modelação Da Circulação Oceânica No Arquipélago de Cabo Verde.” Instituto Superior Técnico - Universidade de Lisboa.

Haynes, R., E. D. Barton, and I. Pilling. 1993. “Development, Persistence, and Variability of Upwelling Filaments off the Atlantic Coast of the Iberian Peninsula.” *Journal of Geophysical Research* 98(C12):22681.

Haynes, R. and Eric D. Barton. 1990. “A Poleward Flow along the Atlantic Coast of the Iberian Peninsula.” *Journal of Geophysical Research* 95:425–41.

Hoinka, By Klaus P. and Manuel D. E. Castro. 2003. “The Iberian Peninsula Thermal Low.” 1491–1511.

http://www.argo.ucsd.edu/How_Argo_floats.html. “http://www.argo.ucsd.edu/How_Argo_floats.html.” Retrieved October 8, 2017 (http://www.argo.ucsd.edu/How_Argo_floats.html).

Hurrell, J. W., Y. Kushnir, and G. Ottersen. 2003. “ An Overview of the North Atlantic Oscillation, The North Atlantic Oscillation.” *Climatic Significance and Environmental Impact* (134):1–35.

Kostianoy, A. G. and A. G. Zatsepin. 1996. “MARINE The West African Coastal Upwelling Filaments and Cross-Frontal Water Exchange Conditioned by Them.” 7963(95).

Leendertsee, J.; Liu, S. 1978. “A Three-Dimensional Turbulent Energy Model for Non-Homogeneous Estuaries and Coastal Sea Systems.” *Nihoul J. (Eds.), Hydrodynamics of Estuaries and Fjords, Elsevier* 387–405.

Lentz, Seteven. 2004. “The Response of Buoyant Coastal Plumes to Upwelling-Favorable Winds *.” 2458–69.

Martins, F., R. Neves, and P. C. Leitão. 1998. “A Three-Dimensional Hydrodynamic Model with Generic Vertical Coordinate.” *Hydro-Informatics* (98):1403–10.

Martins, Flávio, Paulo Leitão, Adélio Silva, and Ramiro Neves. 2001. “3D Modelling in the Sado Estuary Using a New Generic Vertical Discretization Approach.” *Oceanologica Acta* 24:51–62. Retrieved (http://linkinghub.elsevier.com/retrieve/pii/S0399178401000925).

McCartney, M. T. 1992. “The Subpolar Mode Water of the North Atlantic Ocean.” *Journal of Physical Oceanography* 12:1169– 1188.

Nogueira, E., F. F. Pérez, and A. F. Ríos. 1997. “Seasonal Patterns and Long-Term Trends in an Estuarine Upwelling Ecosystem (Ría de Vigo, NW Spain).” *Estuarine, Coastal and Shelf Science* 44(3):285–300. Retrieved (http://linkinghub.elsevier.com/retrieve/pii/S0272771496901195).

Otero, P., M. Ruiz-villarreal, and A. Peliz. 2008. “Variability of River Plumes off Northwest Iberia in Response to Wind Events.” 72:238–55.

Paillet, J. A. 1996. “Oceanic Ventilation in the Eastern North Atlantic.” *Journal of Physical Oceanography 26* 2036– 2052.

Peliz, Álvaro, Teresa L. Rosa, A.Miguel P. Santos, and Joaquim L. Pissarra. 2002. “Fronts, Jets, and Counter-Flows in the Western Iberian Upwelling System.” *Journal of Marine Systems* 35(1–2):61–77.

Pelíz, A., T. L. Rosa, a M. P. Santos, and J. L. Pissarra. 2002. “Fronts, Currents and Couner-Flows in the Western Iberian Upwelling System.” *Journal of Marine Systems* 35:61–77.

Peliz, Álvaro, Jesús Dubert, A.Miguel P. Santos, Paulo B. Oliveira, and Bernard Le Cann. 2005. “Winter Upper Ocean Circulation in the Western Iberian Basin - Fronts, Eddies and Poleward Flows: An Overview.” *Deep-Sea Research Part I: Oceanographic Research Papers* 52(4):621–46.

Perez, Fiz F. Mintrop, L. Llinás, O., Dávila, Melchor, Castro, C., Alvarez, M., Kortzinger, A. Casiano, M. Rueda, M., Ríos, Aida. 2001. “Mixing Analysis of Nutrients , Oxygen and Inorganic Carbon in the Canary Islands Region.” *Journal of Marine Systems* 28:183–201.

Pingree, R. D. and B. Le Cann. 1990. “Structure, Strength and Seasonality of the Slope Currents in the Bay of Biscay Region.” *J. Mar. Biol. Ass. U.K.* 70:857–85.

R, Lars Petter and Xiao Bing Shi. 1999. “A Numerical Study of the Dynamics and Energetics of Cool Filaments , Jets , and Eddies off the Iberian Peninsula Lars Petter I and Xiao Topographic and / or Coastline Irregularities , Transport in the Upper Ocean , Leading to a Persistent Physical Process.” 104.

Ramp, Steven R., Jessen, P., Brink, K., Niiler, P., Daggett, F., Best. F. 1991. “The Physical Structure of Cold Filaments Near Point Arena , California , During June 1987.” 96(91).

Relvas, Paulo et al. 2007. “Physical Oceanography of the Western Iberia Ecosystem: Latest Views and Challenges.” *Progress in Oceanography* 74(2–3):149–73.

Ribeiro, Ana C., Álvaro Peliz, and A.Miguel P. Santos. 2005. “A Study of the Response of Chlorophyll-a Biomass to a Winter Upwelling Event off Western Iberia Using SeaWiFS and in Situ Data.” *Journal of Marine Systems* 53(1–4):87–107.

Rossi, Vincent et al. 2013. “Cross-Shelf Variability in the Iberian Peninsula Upwelling System: Impact of a Mesoscale Filament.” *Continental Shelf Research* 59:97–114.

Sanctuary, Cordell. n.d. “Cordell Bank National Marine Sanctuary.” Retrieved October 8, 2017 (http://cordellbank.noaa.gov/environment/seasons.html).

Santos, A. M. P., Peliza, A., Dubertb , J., Oliveira, P.B., Angelico,M.M.,Ré,P. 2004. “Impact of a Winter Upwelling Event on the Distribution and Transport of Sardine (Sardina Pilchardus) Eggs and Larvae off Western Iberia: A Retention Mechanism.” *Continental Shelf Research* 24(2):149–65.

Santos, A.Miguel P., Chacharo, A., Santos, A., Moita, T., Oliveira, P.B., Peliz, A., Pedro Ré. 2007. “Physical-Biological Interactions in the Life History of Small Pelagic Fish in the Western Iberia Upwelling Ecosystem.” *Progress in Oceanography* 74(2–3):192–209.

Santos, Aires J. P., João Nogueira, and Helder Martins. 2005. “Survival of Sardine Larvae off the Atlantic Portuguese Coast: A Preliminary Numerical Study.” *ICES Journal of Marine Science* 62(4):634–44.

Strub, P. T. E. D., P.Michael Kosro, and Adriana Huyer. 1991. “The Nature of the Cold Filaments in the California Current System.” 96.

Torres,R.; Barton, E. 2007. “Onset of the Iberian Upwelling along the Galician Coast.” *Continental Shelf Research* 27:1759–78.

Trancoso, A. R. 2005. “Modelling Macroalgae Using a 3D Hydrodynamic-Ecological Model in a Shallow, Temperate Estuary.” *Ecological Modelling* 232–46.

Visbeck, Martin et al. 2003. “6 . The Oceans Response to North Atlantic Oscillation Variability.” *Atlantic* 15(8):2581–97. Retrieved (http://www.hydrol-earth-syst-sci.net/15/2581/2011/).

Woster, W.; Reid, Jr. 1963. “Eastern Boundary Currents.” *M.N. Hill (Ed.) The Sea* 2:253–80.